energies

MDPI

Article

Particles Morphology of Mechanically Generated Oil Mist Mixtures of SAE 40 Grade Lubricating Oil with Diesel Oil in the Context of Explosion Risk in the Crankcase of a Marine Engine

Leszek Chybowski [1,*], Marcin Szczepanek [2,*], Katarzyna Gawdzińska [1] and Oleh Klyus [3]

[1] Department of Machine Construction and Materials, Faculty of Marine Engineering, Maritime University of Szczecin, ul. Willowa 2, 71-650 Szczecin, Poland; k.gawdzinska@pm.szczecin.pl
[2] Department of Power Engineering, Faculty of Marine Engineering, Maritime University of Szczecin, ul. Willowa 2, 71-650 Szczecin, Poland
[3] Department of Marine Power Plants, Faculty of Marine Engineering, Maritime University of Szczecin, ul. Willowa 2, 71-650 Szczecin, Poland; o.klyus@pm.szczecin.pl
* Correspondence: l.chybowski@pm.szczecin.pl (L.C.); m.szczepanek@pm.szczecin.pl (M.S.); Tel.: +48-91-48-09-412 (L.C.); +48-91-48-09-376 (M.S.)

Abstract: This article presents research results on mechanically generated oil mists. The research was carried out for oil mixtures for the Agip/Eni Cladium 120 SAE 40 API CF oil for industrial and marine engines diluted with diesel oil Orlen Efecta Diesel Bio at diesel oil concentrations of 2%, 5%, 10%, 20%, and 50% m/m. Pure lubricating oil and pure diesel oil were also tested. Droplet size distributions were determined for the reference moment at which residual discrepancies R between the measurement data and the sprayed pure diesel oil calculation model obtained the lowest value. For mechanically generated oil mists, the light transmission coefficient through the oil mist T, the specific surface area of the oil mist SSA, and the volumetric share of drops $D_V(V\%)$ for 10%, 50%, and 90% of the total volume of the generated oil mist were determined. The span of the volumetric distributions of droplet sizes $SPAN$, Sauter mean diameter $D_{[3,2]}$, De Brouckere mean diameter $D_{[4,3]}$, the volumetric and mass percentage of droplets with diameters $\leq$5 µm (diameters necessary for a crankcase explosion), the minimum difference between the measurement results, and the calculation model used by the residual error measuring device were determined. The best fit in each measurement cycle (the smallest R value was analyzed. For specific indicators, correlations with diesel oil levels in the mixture were determined using the Pearson r_{XY} linear correlation coefficient. Those results confirmed an increase in smaller-diameter droplets, an increase in the number of droplets with diameters up to 5 µm, and an increase in the span of the oil mist droplet diameter distribution with additional diesel oil. This confirmed a relationship between an increased lubricating oil dilution and an increased explosion risk in the crankcase.

Keywords: crankcase explosion; lubricating oil properties; oil dilution with distillation fuel; mechanical spray generation; laser diffraction; oil mist particle distribution

Citation: Chybowski, L.; Szczepanek, M.; Gawdzińska, K.; Klyus, O. Particles Morphology of Mechanically Generated Oil Mist Mixtures of SAE 40 Grade Lubricating Oil with Diesel Oil in the Context of Explosion Risk in the Crankcase of a Marine Engine. *Energies* **2023**, *16*, 3915. https://doi.org/10.3390/en16093915

Academic Editor: Anastassios M. Stamatelos

Received: 14 April 2023
Revised: 1 May 2023
Accepted: 4 May 2023
Published: 5 May 2023

1. Introduction

Combustion engines are the primary source of mechanical energy in transportation and many industries, and are the primary movers of marine propulsion systems [1–3]. They also commonly supply marine generator sets [4–6]. Fire and explosions represent threats to ships and offshore facilities during their operation [7–9]. The most dangerous are explosions in the crankcases of internal combustion engines [10–12]. Such explosions are very dangerous for engine construction and the environment (crew).

The causes and analyses of crankcase explosions have received significant research attention for quite some time [13–15]. This research was conducted alongside general explosion analyses [16–18]. One of the first people to analyze this subject was Minkhorst [19],

who, in 1957, published an in-depth literary analysis of crankcase explosions in the context of a four-engine explosion on board the ocean liner m/v Reina del Pacifico on 11 August 1947 [20]. This explosion killed 28 people and injured 23 others. This event resulted in the development and dissemination of the use of explosion valves and oil mist detectors (OMD) [21]. Initially, these technologies mitigated the effects of possible explosions. However, people later began to think about the causes of explosions and how to prevent them. Crankcase explosions that occurred in subsequent years were the subject of further research [20]. Exemplary consequences are shown in Figure 1 [22].

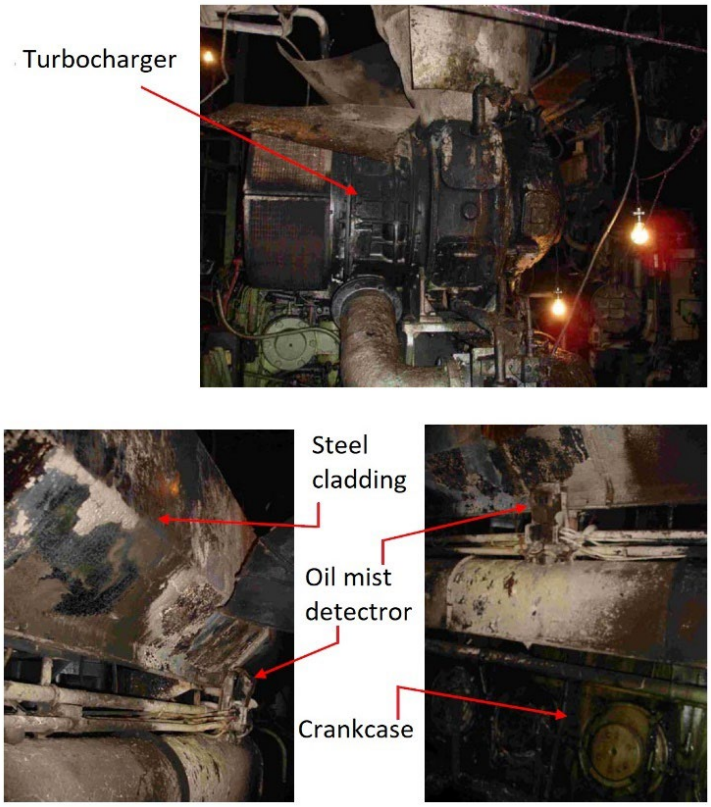

Figure 1. View of the main engine after a fire in the engine room that resulted from an explosion in the crankcase of the An Tai Jiang ship (Hong Kong Marine Accident Investigation Section, 2009).

Figure 1 shows the selected effects of an explosion in the main engine crankcase of the oil tanker An Tai Jiang on 9 January 2009. The explosion initiated a fire in the engine room that spread to the accommodation spaces. Crew accommodations and the engine room suffered severe damage. The explosion killed the third engineer and a motorman inside the engine room, and another motorman was lost at sea after falling into the water.

Causes and prevention of crankcase explosions were addressed in several publications [23–25]. In Ref. [26], the authors reported the statistical analysis results of 99 explosions (between 1972 and 2018) in the crankcases of main engines. This publication confirmed the continued topicality of the issue, and that despite the OMD protections in place, they can happen.

Among the preventative methods to reduce the risk of crankcase explosions of trunk piston engines is periodic testing of the lubricating oils based on ignition temperature and oil viscosity changes as a way to rapidly detect dilution of the engine's circulating lubricating oil with distillation fuel [27]. The change in the flash point temperature of the selected lubricating oils diluted with diesel oil is shown in Figure 2 (based on [28,29]). In contrast, the dilution of lubricating oil with diesel oil unquestionably affects these indicators. Still, the effect of lubricating oil dilution on the explosion risk remains debatable [28].

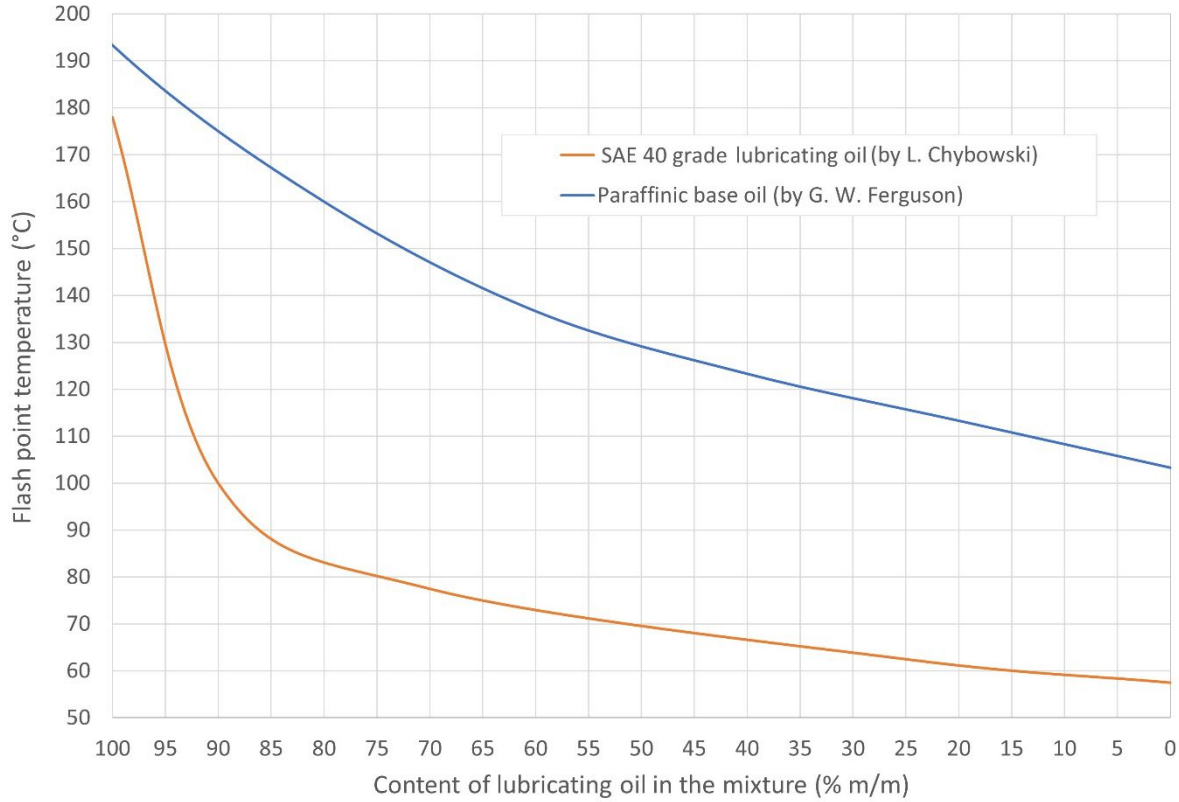

Figure 2. The flash point temperature change for selected mixtures of lubricating and diesel oils at different lubricating oil concentrations in the mixture.

The publication of CIMAC (the International Council on Combustion Engines) Working Group 8 "Marine Lubricants" [30] entitled "Guideline on the relevance of lubrication flash point in connection with crankcase explosions" concluded that "flash point testing of lubricating oils as an accurate or early indicator of the potential risk of a crankcase explosion has not been proven, and so it is no longer recommended for this purpose". Ferguson drew similar conclusions [29], and as a result of his experiment, despite the ignition temperature decrease of the mixture with increased lubricating oil dilution, he stated that the relationship between contamination of lubricating oil with diesel oil and the impact of this contamination on the increased risk of explosion in the engine crankcase could not be proven.

The conclusions drawn by CIMAC and Ferguson contradict observations made by other authors [31]. Some reported that 2–5% of diesel oil in lubricating oil may be dangerous for the engine [32]. Hence, in our opinion, a holistic investigation of this topic is crucial, especially considering that these conclusions are contradictory to others [33,34].

In Ref. [35], the direct impact of lubricating oil contamination with diesel oil on oil volatility was presented. On the other hand, the authors confirmed a change in the rheological properties of lubricating and diesel oil mixtures [28]. At diesel oil concentrations above 10%, the oil film of the tribological pair elements separated by the tested oil was broken. The tests were carried out on a high-frequency reciprocating rig (HFFR). In order to obtain a complete account of lubricating oil dilution impacts on the explosion risk, those works were extended, following the assumptions of Ref. [36], with an analysis of lubricating and diesel oil particle mixture morphologies, and represents the subject of this article.

Therefore, the article supplements other publications by presenting the results of previous research on multi-aspect assessment of the contamination impact of circulating lubricating oil with distillate fuel and the impact of this contamination on the crankcase explosion risk in a marine engine. In addition to previous analyses of the rheological, ignition, and anti-wear properties of lubricating oils, this article presents the effect of

lubricating oil dilution by diesel oil on the morphological characteristics of oil mist droplets produced by the mixtures (study of structure and/or form of droplets [8–10]).

The activities of international institutions related to the safety of maritime transport resulted in improved legal regulations surrounding the operational safety of marine engines, which included minimizing the risk of explosion in the engine crankcase.

The guidelines included in the International Association of Classification Societies (IACS) [37] and detailed regulations of individual classification societies are mentioned here. The IACS guidelines for crankcase protection result from provisions in the SOLAS Convention (Chapter II-1, Regulations 27-2 and 27-4) [38]. The IACS crankcase protection guidelines are contained in unified requirements in sections *M9* (revision 3, correction 2, dated 2 September 2007) and M10 (revision 4, dated 4 July 2013).

IACS regulations state that marine engines with a rated power >2250 kW or a cylinder diameter of >300 mm must be equipped with an oil mist detection system like an OMD, a crank-piston bearing temperature measurement system, or other equivalent devices [37]. Slow-speed engines must be equipped with an alarm system and an automatic emergency load reduction system SLD, whereas medium- and high-speed engines must be equipped with an alarm system and an automatic emergency stop system SHD.

Currently, some new methods for bearing and crankshaft condition monitoring are being developed [39–41], in addition to the application of automatic engine room fire detection systems [42–44].

The content concerning the protection of marine engines is also detailed in the codes developed by the International Maritime Organization (IMO) [45]. This applies to gas-fueled engines and gas dual-fuel engines. According to International Gas Carrier Code (IGC) guidelines, trunk piston engines fueled with gas and dual-fuel engines (gas and liquid fuel) must be equipped with OMDs [46]. However, this applies to LNG carriers, not all vessels equipped with gas or dual-fuel engines. Regulations for other ships equipped with gas-fueled engines are listed in the International Code of Safety for Ships Using Gases of Other Low-Flashpoint Fuels (IGF). Yet, this document only indicates the need to assess the risk and apply appropriate safeguards if fuel enters the crankcase of trunk piston engines (in Ref. [11] in Annex 4). Specific guidelines may be more stringent, considering the regulations of a given country or a classification society [47].

Mist detectors work on an optical principle. The first OMD using light absorption was introduced in the 1960s by British companies specializing in fire protection [48]. Currently, five manufacturers supply most detectors [49], and Figure 3 gives their market share.

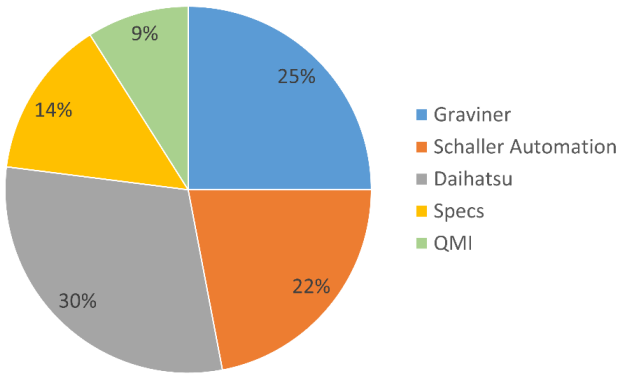

Figure 3. Percentage of market share for major suppliers of oil mist detectors (Hamied, 2016; Chybowski, 2022).

The first devices were too sensitive and often generated false alarms, which caused the engine room staff to mistrust their operation. The devices were subsequently improved by introducing more reliable light sources and systems using nephelometric measurements. Time measurements and oil mist detection were shortened significantly with greatly improved accuracy. Current OMDs generate an acoustic and visual alarm at oil mist con-

centrations between 1.25–2.00 mg/dm^3 (mg/L), i.e., well below the lower explosive level of 47 mg/dm^3 (mg/L) [50,51].

Currently, there are two basic methods of oil mist detection based on the analysis of a gas sample taken from the crankcase. These methods use sample (opaque measurement), light absorption (visible or infrared), or the sample light scattering method (nephelometric detectors). Absorption was used in the first OMD by Graviner and Daihatsu and is used currently in Visatron devices by Schaller Automation, while nephelometric detectors are produced by Kidde-Graviner in the MK series and detectors manufactured by Specs Quality Monitoring Instrument—QMI and Daihatsu, the MD-SX series.

Oil drops floating in the crankcase atmosphere have diameters ~200 µm, and to produce a fine explosive mist [52], the droplets must have diameters between 5–6 µm [53,54]. The lower explosion limit for a mixture of oil and air is 47–50 mg/dm^3 (mg/L) [55,56].

Oil mists form in the crankcase in one of two ways—thermally or mechanically [57].

A thermally generated mist forms at sufficiently high temperatures [58–60] when the evaporating oil mixes with air and circulates in a closed volume inside the crankcase [61]. It condenses to form an aerosol at temperatures below the evaporation temperature [62]. Oil droplets in thermally generated mists typically have diameters between 0.1–10 µm. The heat source to generate engine crankcase mists comes from so-called hot spots related to local overheating of engine components (seizing crank bearings [22,63,64], an external heat source—fire in the engine room [11,65–67], and additionally damaged stuffing box or fire in scavenging spaces in crosshead engines [10]). The intensity of oil mist generation is affected by the hot spot temperature and the volatility of the oil itself. Figure 4 shows the relationship between lubricating with diesel oil dilution and the mixture volatility increase (boiling point reduction) presented in previous studies [35]. Those results showed that the boiling point decrease in the lubricating/diesel oil mixture at higher lubricating oil dilutions translated into additional evaporation of that mixture from the hot spot, which increased the amount of thermally generated oil mist.

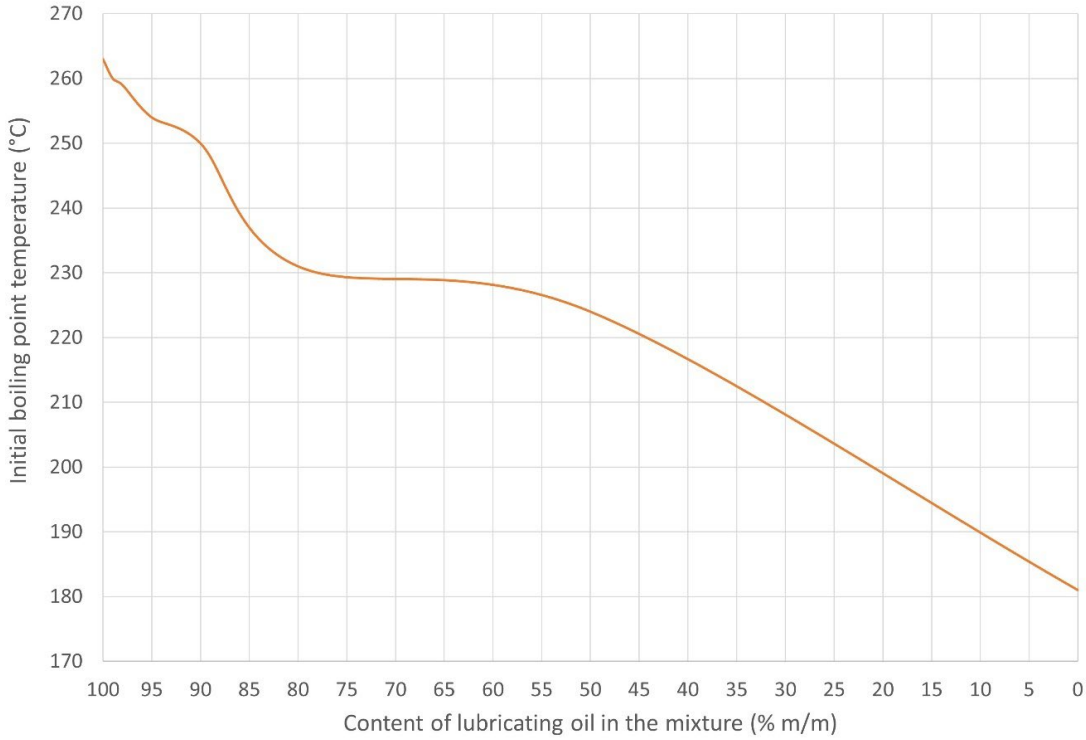

Figure 4. Changes to the initial boiling point temperature for selected mixtures of SAE 40 lubricating oil with diesel oil at different lubricating oil concentrations in the mixture (Chybowski, 2022).

The second method of crankcase mist formation is mechanical generation. This method is analogous to spraying fuel through an injector [68]. This results in a wide range of droplet diameters, with most above 10 μm [69]. Mechanical mist generation in the crankcase is primarily caused by the tribological piston–piston rings–cylinder liner systems. During operation, oil is extruded from between the cooperating elements of these tribological pairs into the crankcase [70]. This comes from both pressure blow-offs from the combustion chambers [71] (often associated with the poor technical condition of the piston rings [72]) and oil extrusion resulting from the dynamics of the piston rings [73] and their cooperation with the piston and cylinder liner [74] (the so-called oil pumping through the piston rings [75]).

In both cases, the droplet size distribution from evaporation and atomization maintains an approximately constant tendency compared to differences in droplet size that depend on the heater or atomizer distance, where the size distribution is recorded and analyzed [76,77]. Droplet size differences vary depending on the mist-forming substance [52,53].

In accordance with IACS guidelines (M67 8.1.1.2 in Ref. [37]) on the OMD test, the validation of oil mist detection devices must be carried out using single-grade SAE 40 mineral oil or its equivalent; the mist should have an average (or arithmetic mean) diameter <5 μm.

In practice, OMDs are often tested indirectly using a chemically generated mist with a manual pump, e.g., ethylenediamine and acetic acid [78], using a manual pump or oil mist of reference oil thermally generated by dedicated oil mist generators, e.g., by Schaller Automation [57] or Concept smoke systems [79].

Thermal mist generators, however, produce mist with specific droplet sizes of liquid suspended in the air, desirable for OMD testing. Moreover, such generators do not control the average diameter size (or not very well) or the distribution of the droplet diameters in the oil mist. Moreover, they usually do not allow testing small (analyzed in laboratory conditions) amounts of liquids from which oil mist is generated.

Mechanical generation of oil mist was chosen as it offers the best control of the oil mixture to test mists with various dilutions of the lubricating oil with diesel oil. Moreover, such an approach enables conclusions to be drawn from a comparative analysis of the droplet size distribution produced from various liquids (lubricating and diesel oil mixtures with different component mass fractions) produced in the most similar conditions in each measurement cycle.

The authors hypothesized that increased diesel oil contamination would increase the share of droplets with smaller diameters. For this purpose, a stream of oil sprayed by the injector was tested analogically to similar tests carried out for fuels [80]. The number of droplets with diameters up to 5 μm, indicated in the IACS guidelines, was determined [37]. This approach made it possible to draw conclusions regarding the relative changes in the number of droplets of the desired size to initiate an explosion that depended on the oil mist chemical composition when the lubricating oil and diesel oil types used in the dilution were known. This approach determined the relative change in the characteristics of the generated mist for different diesel oil levels in the lubricating oil.

2. Materials and Methods

Following the IACS guidelines, a single-grade SAE 40 viscosity oil [81] and quality category API CD [82], intended for marine, traction, and industrial engines Agip/Eni Cladium 120 SAE 40 API CF [83], was tested in accordance with IACS guidelines. Appendix A contains the requirements for the lubricating oil used. Orlen Efecta Diesel Bio diesel oil [84] diluted the lubricating oils and met the Regulation of the Minister of Economy requirements for liquid fuels (RMG) [85] and the ZN-ORLEN-5:2019 standard [86].

Samples of pure lubricating oil, pure diesel oil, and lubricating oil contaminated with 2%, 5%, 10%, 20%, and 50% diesel oil in the mixture were analyzed. Of course, in typical operating conditions, concentrations of diesel oil in the lubricating oil are usually low and do not exceed 2–5% in practice, which some researchers consider requires preventive action.

Therefore, in response to some works [29,30] that stated that diluting lubricating oil with diesel oil, even at high concentrations of diesel oil (e.g., 20% diesel oil), does not increase the risk of explosion in the crankcase, an experiment was undertaken over the full range of concentrations (from pure lubricating oil to pure diesel oil). Additionally, it should be noted that the tests were carried out over the full range of diesel oil concentrations in the lubricating oil, which aimed to capture certain regularities and determine the relationships between the change of a given parameter and the content of diesel oil in the lubricating oil. This approach enabled obtaining of a complete picture of cause-and-effect relationships, and conclusions could be drawn for any other lower concentration or range of diesel oil concentrations in the mixture, including content that does not exceed 30%. For this purpose, the resolution of the tested samples was increased in the range of the low concentrations (i.e., 0%, 2%, 5%, 10%, and 20% of diesel oil in the lubricating oil). Concentrations above 10% m/m of diesel oil significantly exceed the amounts of contamination of diesel lubricating oil encountered in standard operating practice. However, the study aimed to determine the relationship between the oil mist droplet size distribution and the amount of diesel oil in the mixture.

To fully determine the relationship between the lubricating oil dilution, the morphological characteristics of the oil mist particles, and the correlation between the mist droplet size distribution and the amount of pure lubricating oil in the mixture, the mixtures were tested over a wide concentration range. The selection of diesel oil concentrations was dictated by the need to maximize the number of measurements at low diesel oil concentrations (occurring in operational practice), and to determine the nature of changes over a broad concentration range. Therefore, high-level samples (20%, 50% m/m, and 100%—pure diesel oil) of diesel oil were also tested.

The selection of measurement points sought to maintain interconnectivity between these test results and previously published observations [35] and their rheological, anti-wear, and ignition properties [28]. This approach made it easier to draw broad conclusions about the effect of diesel oil on lubricating oil properties.

The oil samples were heated to 80 °C to lower the viscosity of the liquid and ensure spraying the samples by the injector on the test stand would produce an oil mist. Pure lubricating oils and lubricating oil mixtures with low levels of diesel oil have high viscosities at room temperature (in this case, 20 °C), which made it impossible for the injector to spray samples at room temperature. The SAE 40 class oil mixtures at diesel oil concentrations from 0–20% m/m analyzed at 40 °C had viscosity values between 40–160 mm^2/s (cSt).

High viscosities prevented proper spraying and caused excessive pressure increases in the injection system during testing, which could damage the injection pump. The viscosity was lowered to avoid this damage, as in residual fuel injection systems, to the level recommended by the engine/injection equipment manufacturer. For marine and industrial engines, the recommended fuel viscosity (for high-viscosity fuels at a reference temperature of 50 °C [87–89]) should be 10–15 mm^2/s, which requires heating the fuel fed into the engine (the so-called viscosity control system) [64,65]. To maintain similar injection conditions for all samples during mechanical generation, the maximum oil viscosity fed into the atomizer should not exceed 20 mm^2/s, and the average kinematic viscosity of all tested samples should be ~11 mm^2/s (viscosity deviations from the average should not be greater than ± 9 mm^2/s). Such conditions were ensured by appropriately heating the oil samples to 80 °C.

The physical and chemical properties of pure lubricating oil and diesel oil are presented in Tables 1 and 2, respectively.

Table 1. Manufacturer-declared and measured physicochemical properties of Agip/Eni Cladium 120 API CF lubricating oil used in tests.

Oil	Specification	Declared by the Manufacturer [83,90,91]	Measured Value [28]
Agip/Eni Cladium 120 SAE 40 API CF	Kinematic viscosity (according to EN ISO 3104)	160 mm^2/s at 40 °C 15.7 mm^2/s at 100 °C	159.90 mm^2/s at 40 °C 15.21 mm^2/s at 100 °C
	Viscosity index	100	95.3
	Total base number	12 mg KOH/g	
	Flashpoint (marked in the closed crucible)	235 °C	178 °C
	Pour point	−15 °C	
	Density	900 kg/m^3 at 15 °C	898.44 kg/m^3 at 15 °C

Table 2. Manufacturer-declared and measured physicochemical properties of Orlen Efecta Diesel Bio used in tests.

Specification	Declared by the Manufacturer [84]	Measured Value [28]
Cetane index	≤51	52
Initial boiling point	75–180 °C	181 °C
Boiling temperature range	95% vol. distils to 360 °C	
Flashpoint (determined in a closed crucible)	>56 °C	65 °C
Autoignition temperature (according to DIN51794:2003-05)	approx. 240 °C	
Kinematic viscosity (according to EN ISO 3104)	1.5–4.5 mm^2/s (2.549 mm^2/s) at 40 °C approx. 2.151 mm^2/s at 50 °C	2.897 mm^2/s at 40 °C 2.443 mm^2/s at 50 °C
Density	820-845 kg/m^3 at 15 °C	835.81 kg/m^3 at 15 °C
Relative vapor density	approx. 6 (air = 1)	
Cloud point	−7 °C	
Cold filter plugging point	−8 °C	

Testing results for oil mixture properties used are included in Refs. [22,27] and datasets [66,67]. Density, kinematic viscosity, and dynamic viscosity of the mixtures at 80 °C as a function of lubricating oil dilution with diesel oil are shown in Figures 5–7, respectively [92,93].

Table 3 gives the measurement conditions and injector parameters.

Table 3. External conditions and characteristic parameters during the measurements.

Parameter	Value
Environmental conditions:	
Room air temperature	20 °C
Atmospheric pressure	1007 hPa
Injection parameters:	
Injection pump	WSK PRW3M-00 (PO1B.100S)
The maximum injection pump pressure	40 MPa
Measuring manometer class	0.6
The scale interval value of the measuring manometer	0.4
Atomizer type	D1LMK 148/1
Injected liquid temperature	80 °C
Injector opening pressure	28 MPa
The set dose of the injected liquid	0.6 cm^3
The time from opening the injector to conducting morphology testing of the liquid droplet suspension in the air	0.0748 ms

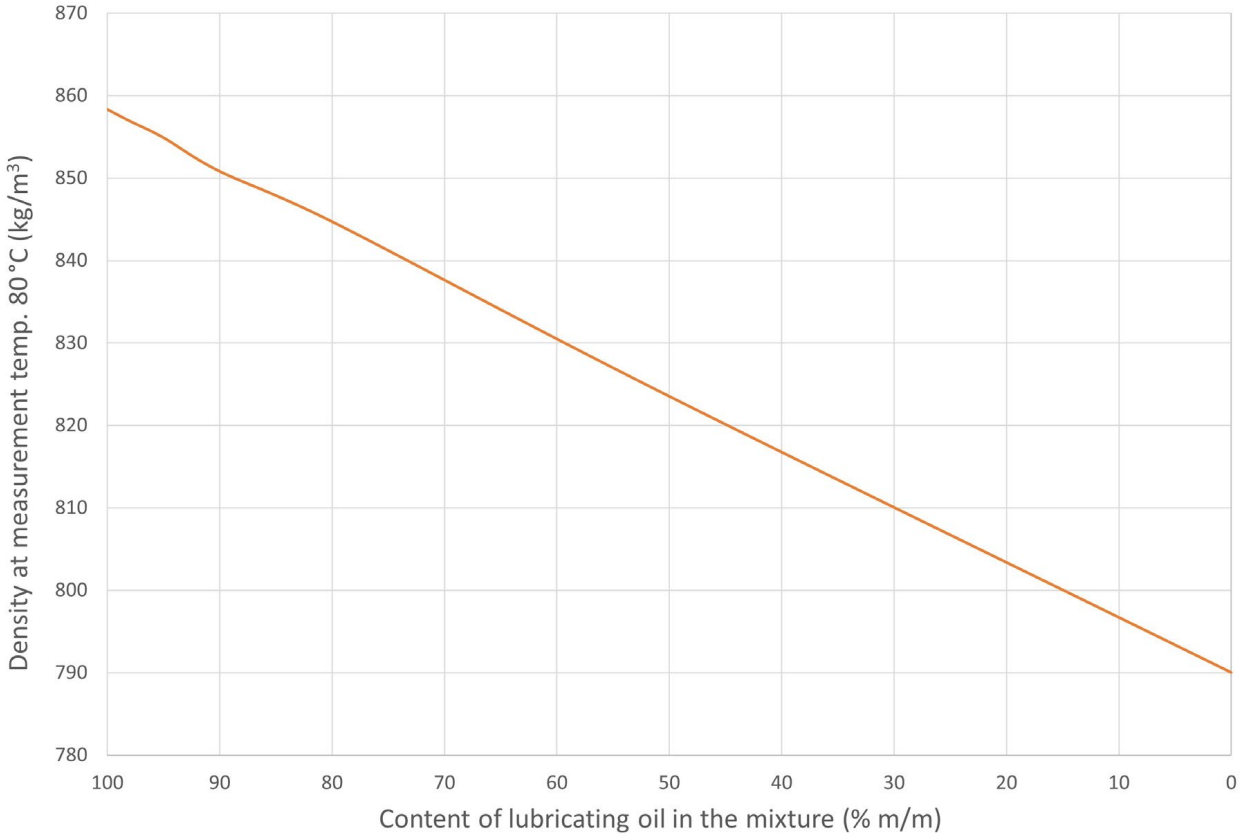

Figure 5. The density of the tested mixtures of SAE 40 oil and diesel oil at 80 °C.

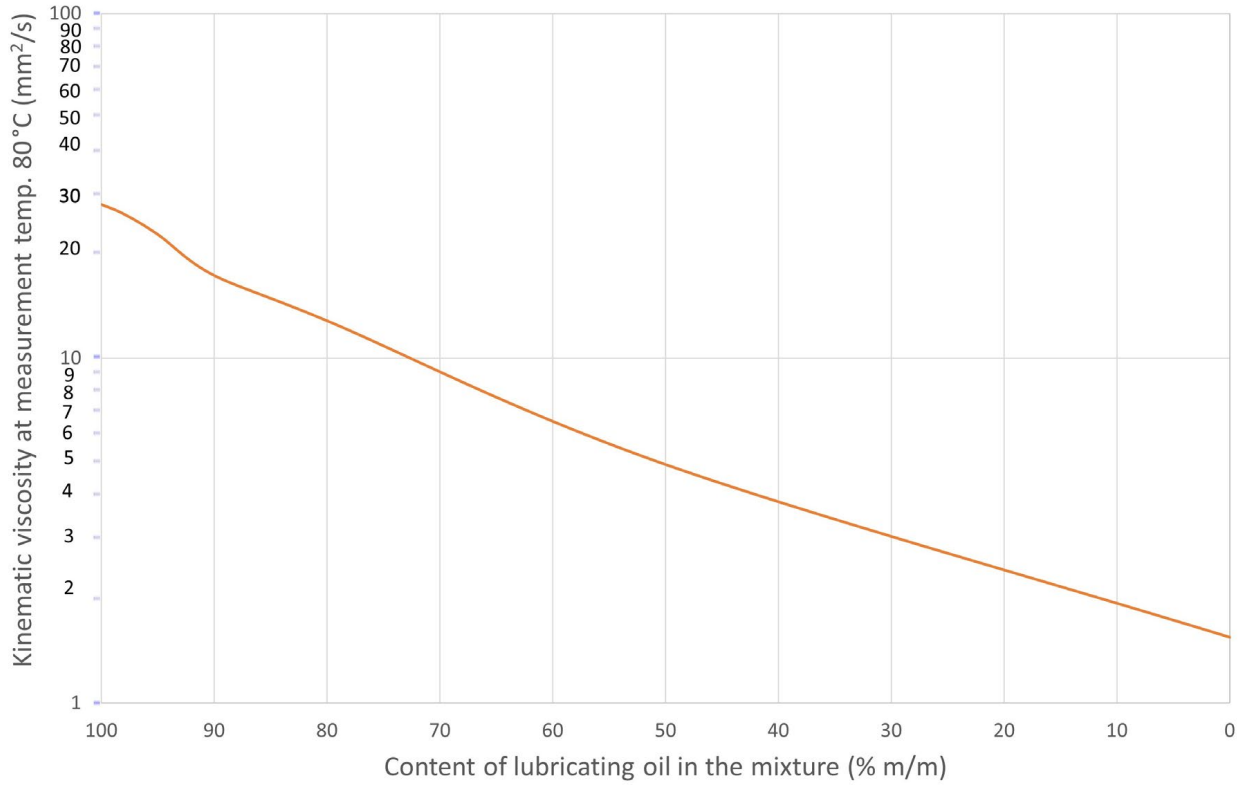

Figure 6. The kinematic viscosity of the tested mixtures of SAE 40 oil and diesel oil at 80 °C.

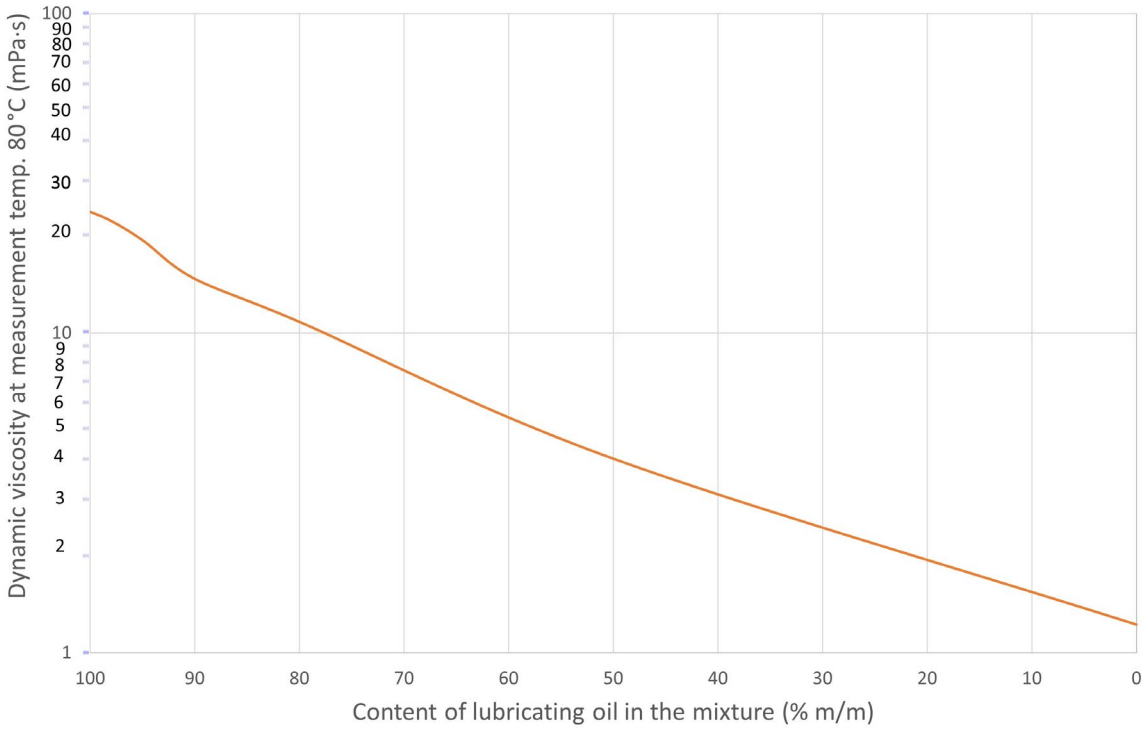

Figure 7. The dynamic viscosity of the tested mixtures of SAE 40 oil and diesel oil at 80 °C.

The crankcase atmosphere composition during the operation of a well-maintained engine approximates the atmosphere of Earth. This applies to both two-stroke and four-stroke engines, engines for liquid fuels, and dual-fuel engines powered by gas [57,94]. For example, the air in the crankcase, depending on the load and engine type, had the following composition [23,42]: 20.3–21.7% v/v O_2, 77.6–79.7% v/v N_2, 1% v/v Ar, <0.7% v/v CO_2, <98 ppm CO, <5 ppm H_2, <2.1% v/v hydrocarbons. With this in mind, spraying lubricating and diesel oil mixtures took place using atmospheric air.

The tests were carried out using a test stand with the Spraytec STP 5000—Open Spray Zetasizer (Malvern Instruments, Worcestershire, United Kingdom) with an 11 CQ-CDL detector apparatus (Malvern Instruments, Worcestershire, United Kingdom), shown in Figure 8. The diagram is prepared based on [95]. Table 4 presents the technical data for the test stand. The device measured the particle size in the spray. Specifically, it measured the distribution of droplet sizes within a spray. Measurement involved the following steps [95]:

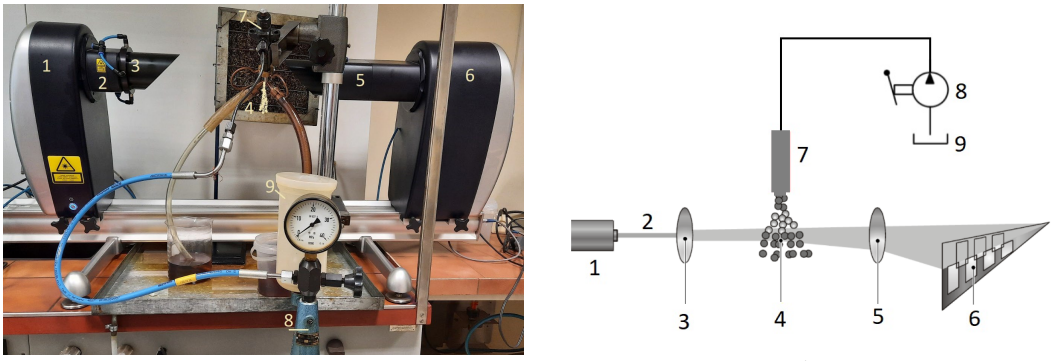

Figure 8. The measurement apparatus used (Spraytec STP 5000—Open Spray Zetasizer): (**a**) device components; (**b**) measurement fundamentals: 1—laser, 2—light beam, 3—collimating lens, 4—tested oil mist, 5—auxiliary focusing lens, 6—beam power detector, 7—injector, 8 high-pressure pump, 9—tank with the tested liquid.

Table 4. Parameters of the measuring device.

Parameter	Value
Instrument	Spraytec STP 5000—Open Spray
Operator	Zetasizer
Detector	11 CQ-CDL
Method of measurement	Laser-diffraction (small-angle scattering)
Optical model	The Mie theory and the Fraunhofer approximation
Aerosol concentration range	Multiple Dispersion Correction System
Light source	Laser type He-Ne, 2 mW, 632.8 nm
Lens	300 mm
Particulate refractive index	1.46 + 0.000i
Dispersant refractive index	1.00
Path length	9.1 mm
Scatter start	1
Scatter end	36
Multiple scatter	On
Scattering threshold	1
Minimum size of particle	0.1 µm
Maximum size of particle	2500 µm
Measurement error	<±1% for Dv(<50% v/v)
Trigger transmission	<90%
Trigger delay	−50 ms

- A previously prepared sample of the test liquid was sprayed using a high-pressure pump and injector.
- The liquid was sprayed in the measurement zone between the Spraytec transmitter and receiver modules.
- The transmitter used a He-Ne (helium-neon) laser that passed through the spray in the measuring zone.
- The light detected was converted into electrical signals by a receiver that detected the light diffraction pattern produced by the sprayed liquid.
- The measurement results were processed and analyzed using dedicated Sprytec analysis software. The light diffraction pattern was analyzed using Mie theory [96,97] and the Fraunhofer approximation [98] to calculate the spray size distribution.

Measuring the droplet size distribution in the mist generated by the fuel injector D1LMK148/1 (PZL-WZM, Jawczyce, Poland) [99], powered by the PRW3M-00 high-pressure pump (WSK, Krakow, Poland) [100], verified the initial hypothesis put forward for different concentrations of diesel oil in the tested lubricating oil. The spray profile adopted in the experiment and the dimensions of the sprayer are shown in Table 5. The cross-section and atomizer hole arrangements are shown in Figure 9.

Table 5. Oil mist spray profile and atomizer dimensions.

Parameter	Value
Spray profile:	
Type	Nozzle spray
The offset of the center of the plume from the lens Z	165 mm
The offset of the center of the plume from the beam P	0 mm
The angle of the spray cone A	13°
The length of the spray cone B	40 mm
Direction of spray angle (0°—vertically upward, 180°—vertically downward)	90°
The geometry of the atomizer slot:	
Atomizer slot diameter d_0	0.34 mm
Atomizer channel length l_0	1.2 mm
Atomizer channel ratio l_0/d_0	3.53
Number of holes	3

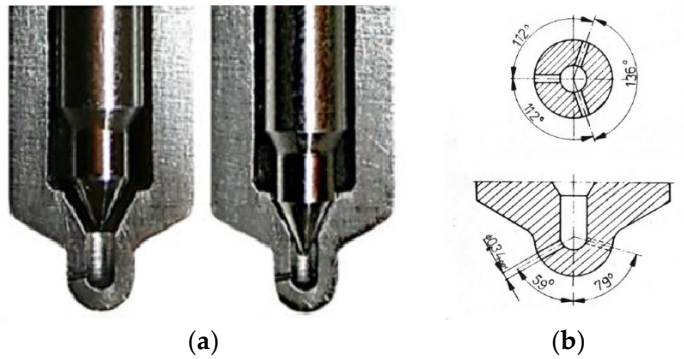

(**a**) (**b**)

Figure 9. The D1LMK148/1 atomizer: (**a**) cross-section in the open (left) and closed (right) positions; (**b**) dimensions and locations of openings in the atomizer nozzle [99].

Each sample was subjected to five tests. Oil mist droplet size distributions were recorded over the entire spraying period. The analysis occurred at time t = 0.0748 ms after opening the injector, at which the lowest values of the average Sauter diameter were recorded for pure diesel fuel (the highest stream atomization). To maintain a consistent relationship, all measurements occurred at that time (a reference value). The analysis used measurement data for a given lubricating/diesel oil composition for a measurement cycle characterized by the most accurate matching of the calculated model with the measurement results (residual R values). The measured data characterized by the lowest R were used and compared. The summary of all experimental data is included in the associated dataset [93]. The R values for each data cycle compared to each other are shown in Figure 10.

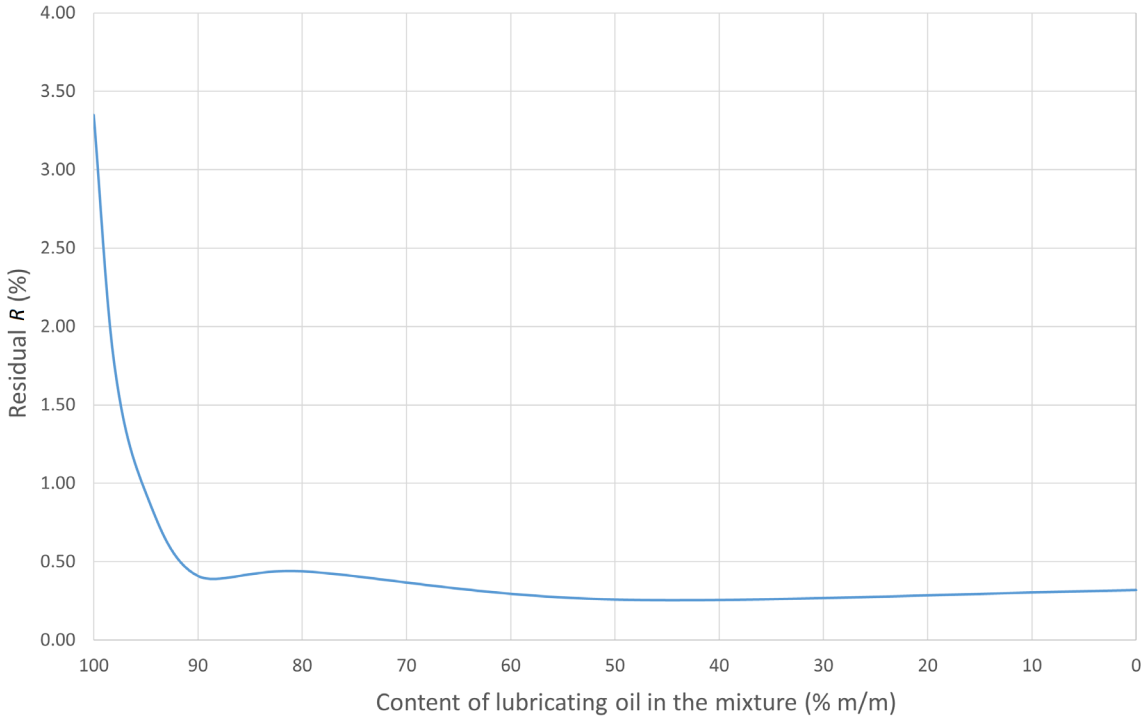

Figure 10. The minimum difference between the measurement results and the calculation model used by the measuring device for the SAE 40 and diesel oil mixtures.

Appendix B presents the mixture droplet size distributions. Cumulative values and volume frequency of droplet diameter distributions for measurement cycles with the smallest R are presented there. A preliminary analysis of the distributions mentioned above showed that with additional diesel oil, the volumetric share in a mixture of droplets with an average diameter and the span of the distribution increased (a decrease in the

maximum value of droplets with a diameter in the distribution mode) and the number of droplets with small diameters increased (a shift of the volume frequency mode value to the left). Detailed conclusions regarding changes in the droplet distribution in the oil mist depending on diesel oil levels in the mixture were drawn based on the detailed distribution characteristics and described later in this article.

For the mechanically generated oil mists, the light transmission coefficient through the oil mist T, the specific surface area of the oil mist SSA, and the volumetric share of droplets $D_V(V\%)$ for 10%, 50%, and 90% of the total mist volume were determined. The relative width of the volumetric distribution of droplet sizes $SPAN$, Sauter mean diameter $D_{[3,2]}$, De Brouckere mean diameter $D_{[4,3]}$, and the volumetric and mass percentage of droplets with diameters $\leq$ the critical droplet diameter of 5 µm were determined.

For specific measured values characterizing the morphology of the oil mist particles, their correlation with the amount of pure lubricating oil in the mixture was determined. Pearson's r_{XY} linear correlation coefficient was used for this purpose:

$$r_{XY} = \frac{\mathrm{cov}(X,Y)}{\sigma_X \cdot \sigma_Y} \quad (1)$$

where: cov(X,Y)—variable covariance X and Y; σ_X and σ_Y—standard deviations of the X and Y variables, respectively.

Based on information in the literature [101,102], the strength of the correlation used was interpreted using the assumptions presented in Table 6.

Table 6. Assumed Pearson correlation coefficient interpretation.

Pearson's r_{XY} Coefficient Value	Interpretation of the Relationship between Two Variables
$0.000 \leq r_{XY} < 0.200$	Very low correlation. No linear relationship.
$0.200 \leq r_{XY} < 0.400$	Low correlation. The relationship is clear.
$0.400 \leq r_{XY} < 0.600$	Moderate correlation. Significant relationship.
$0.600 \leq r_{XY} < 0.800$	High correlation. Significant relationship.
$0.800 \leq r_{XY} \leq 1.000$	Very high correlation. Very high to full relationship.

Light transmission of oil mist T measures the amount of light that reaches the detector F (based on [95,103]):

$$T = \frac{F_0 - F}{F_0} 100\ (\%), \quad (2)$$

Particles block some of the light F_0 upon introduction into the measurement area. Measurement of T and determination of its possible correlation with the amount of lubricating oil in the diesel oil mixtures allow determination of the diesel oil contamination impact on changes for oil mist detector indicators. Pure air has 100% transmission (no spray present) and decreases as the spray concentration increases.

The specific surface area SSA is the total particle area A divided by the total volume V [104]. This figure assumes spherical and non-porous particles.

$$SSA = \frac{A}{V}, \quad (3)$$

D_v(<10% v/v), D_v(<50% v/v), and D_v(<90% v/v) are droplet size percentile distributions by volume, which indicate the maximum droplet size falling within 10%, 50%, or 90% of the droplet sizes of the total mixture volume. The span of the statistical distribution of droplet sizes in the mixture volume was determined using the following relationship [95]:

$$SPAN = \frac{D_V(< 90\%\ v/v) - D_V(< 10\%\ v/v)}{D_V(< 50\%\ v/v)}, \quad (4)$$

According to the ISO 9276-2 standard and the moment-ratio notation, the general definition of mean particle size is described by the following formula [105]:

$$\overline{D}_{[p,q]} = \left(\frac{\sum_{i=1}^{N} n_i D_i^p}{\sum_{i=1}^{N} n_i D_i^q} \right)^{\frac{1}{p-q}}, \quad (5)$$

where: D—particle diameter, i—number of the size class with upper particle size x_i, n—number of particles in i-th size class, N—number of size classes.

There are a number of diameters with different applications depending on their definition [106–108], including the number-weighted mean (arithmetic or linear) $D_{[1,0]}$, surface diameter $D_{[2,0]}$, volume diameter $D_{[3,0]}$, size-weighted mean size diameter $D_{[2,1]}$, size-weighted mean area size diameter $D_{[3,1]}$, surface-weighted (Sauter) mean $D_{[3,2]}$, volume-weighted (De Brouckere) mean $D_{[4,3]}$, and volume-weighted mean area size $D_{[5,3]}$. In the analyses of combustion processes and fuel atomization quality, the $D_{[3,2]}$ [108,109] and $D_{[4,3]}$ [110,111] diameters are primarily used.

The Sauter mean diameter $D_{[3,2]}$ is defined as the average particle size in terms of the volume diameter D_{Vol} and the surface diameter D_S of the particle. For a single molecule, D_V and D_S values are represented as:

$$D_{Vol} = D_{[3,0]} = \sqrt[3]{\frac{6V_p}{\pi}}, \quad (6)$$

$$D_S = D_{[2,0]} = \sqrt{\frac{A_p}{\pi}}, \quad (7)$$

where: Ap—external particle surface area, Vp—particle volume.

The diameter averages are:

$$\overline{D}_{[3,0]} = \left(\frac{\sum_{i=1}^{N} n_i D_i^3}{N} \right)^{\frac{1}{3}}, \quad (8)$$

$$\overline{D}_{[2,0]} = \left(\frac{\sum_{i=1}^{N} n_i D_i^2}{N} \right)^{\frac{1}{2}}, \quad (9)$$

The Sauter diameter is described by the following relationship [81,82]:

$$D_{[3,2]} = \frac{D_V^3}{D_S^2} = \frac{6V_p}{A_P}, \quad (10)$$

The average Sauter diameter is determined according to the following formula:

$$\overline{D}_{[3,2]} = \frac{\left(\overline{D_{[3,0]}}\right)^3}{\left(\overline{D_{[2,0]}}\right)^2} = \frac{\sum_{i=1}^{N} n_i D_i^3}{\sum_{i=1}^{N} n_i D_i^2}, \quad (11)$$

The De Brouckere mean diameter is the mean of a particle size distribution weighted by the volume. This diameter is more sensitive to larger particles, which comprise the largest sample volume. The following relationship determines the average value:

$$\overline{D}_{[4,3]} = \frac{\sum_{i=1}^{N} n_i D_i^4}{\sum_{i=1}^{N} n_i D_i^3}, \quad (12)$$

In order to relate the observations to the requirements of IACS, the mass fraction of droplets with a diameter of less than or equal to 5 µm with a total mass marked as $\%m_{CR}$ in

volume V of the oil to obtain an oil mist was also determined. The mass of droplets with a diameter equal to or smaller than D_{CR} = 5 µm was calculated based on the registered distribution of droplet sizes with different diameters:

$$\%m(D_{CR}) = \rho \cdot \%V(D_{CR}) = \frac{\rho}{V}\int_0^{D_{CR}} VdD = \frac{\rho}{V}\int_0^{5\ \mu m} VdD, \quad (13)$$

where: ρ—density of the oil at the measurement temperature, V—oil mist volume.

3. Results and Discussion

Figure 11 shows the light transmission of the mixtures. At diesel concentrations up to ~20% m/m, light transmission fluctuated around the average of ≈75%. After exceeding 25% m/m of diesel oil in the mixture, light transmission decreased.

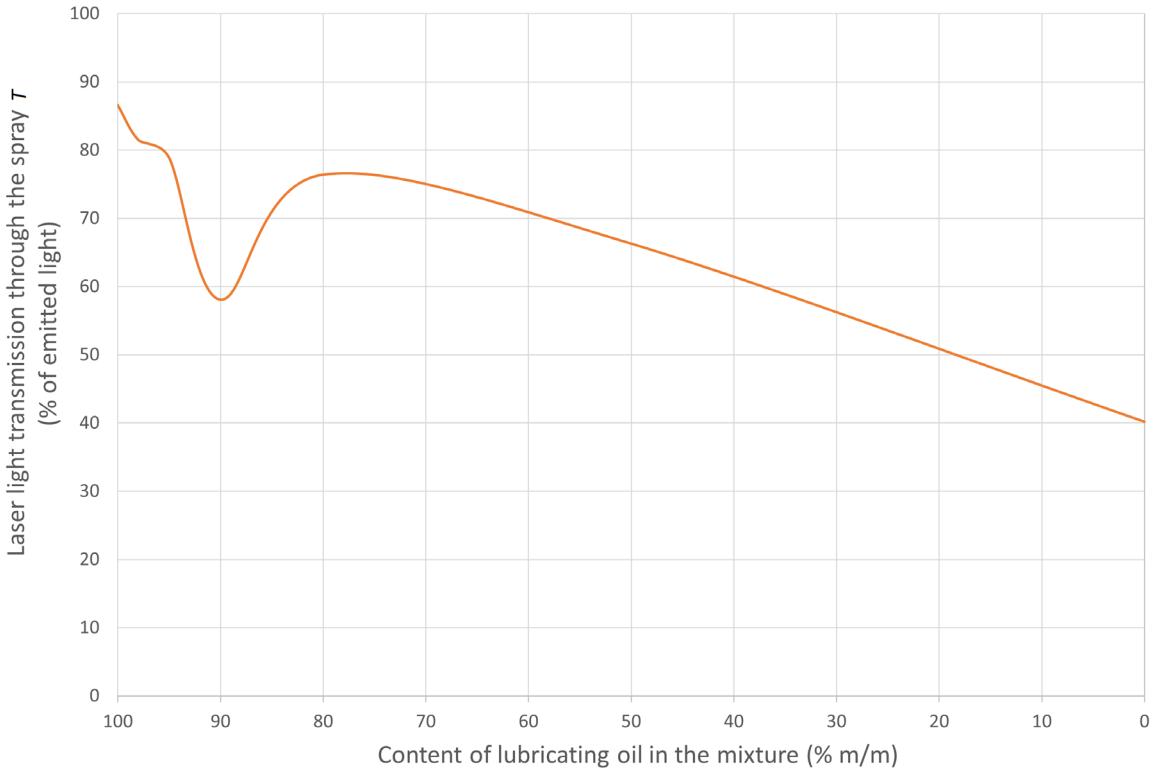

Figure 11. Light transmission of oil mist mixtures of SAE 40 and diesel oils.

The correlation between light transmission of the oil mist and the amount of pure oil in the mixture was very high (0.854). Considering the decreasing nature of the functional relationship presented in Figure 12, OMDs [55] used to protect marine and industrial engines of both the absorption type [11] and the nephelometric type (accounting for the additional reference sensor used) [112] should function seamlessly when monitoring the oil mist level generated from lubricating oil contaminated with diesel oil. For high dilution of the lubricating oil, leveling type OMDs [113] should theoretically generate an alarm faster than for lubricating oils not contaminated with diesel oil. However, for comparator-type OMDs [113], lubricating oil contamination should not affect the measured results.

The results of the analysis of light transmission through the oil mists were compared with the volume spray concentration shown in Figure 12. Changes in concentration for class oil mixtures ranged from 816 to 2938 ppm. At the same time, the spray concentration nature changed in diesel oil concentrations up to 10% m/m and showed fluctuations.

The correlation between the volume concentration and lubricating oil levels in the mixture had a high Pearson coefficient correlation (0.776).

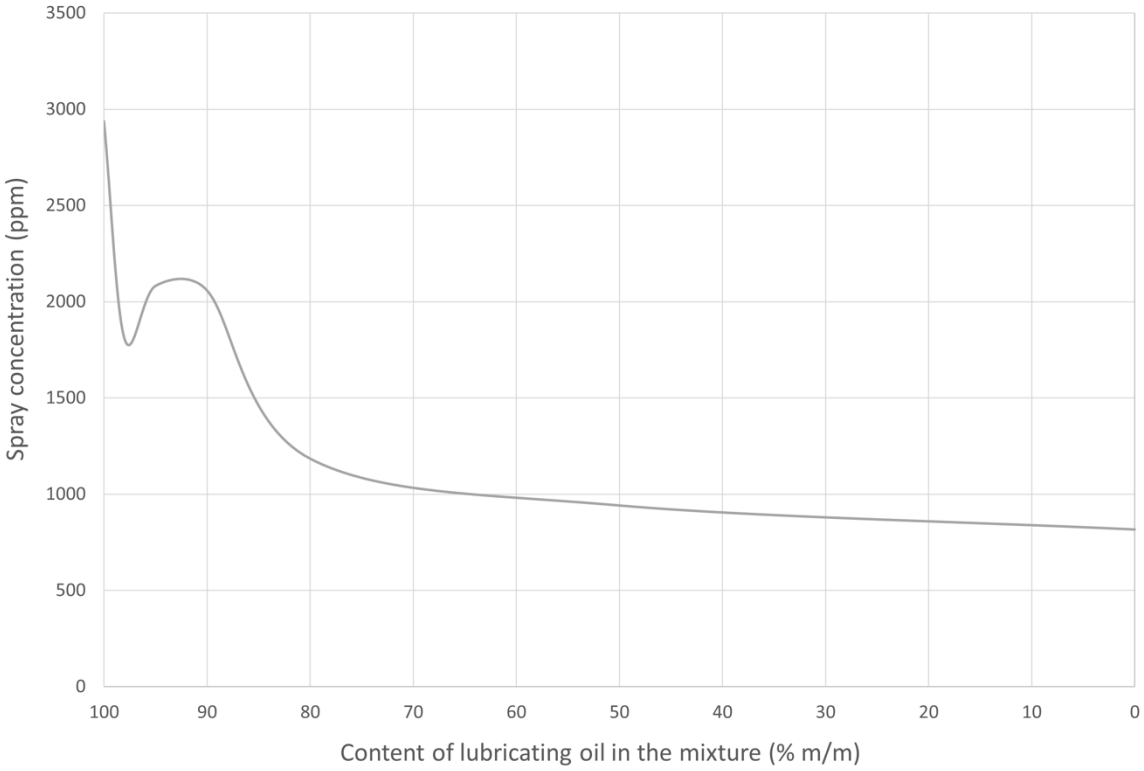

Figure 12. Volume concentration of oil mist droplets of SAE 40 and diesel oil mixtures.

The specific surface area *SSA* of the oil-air aerosols is shown in Figure 13. For diesel oil concentrations up to 20% m/m, slight changes in *SSA* were observed from 0.01–0.05 m^2/cm^3. *SSA* values increased to ~0.14 for pure diesel oil above 20% m/m.

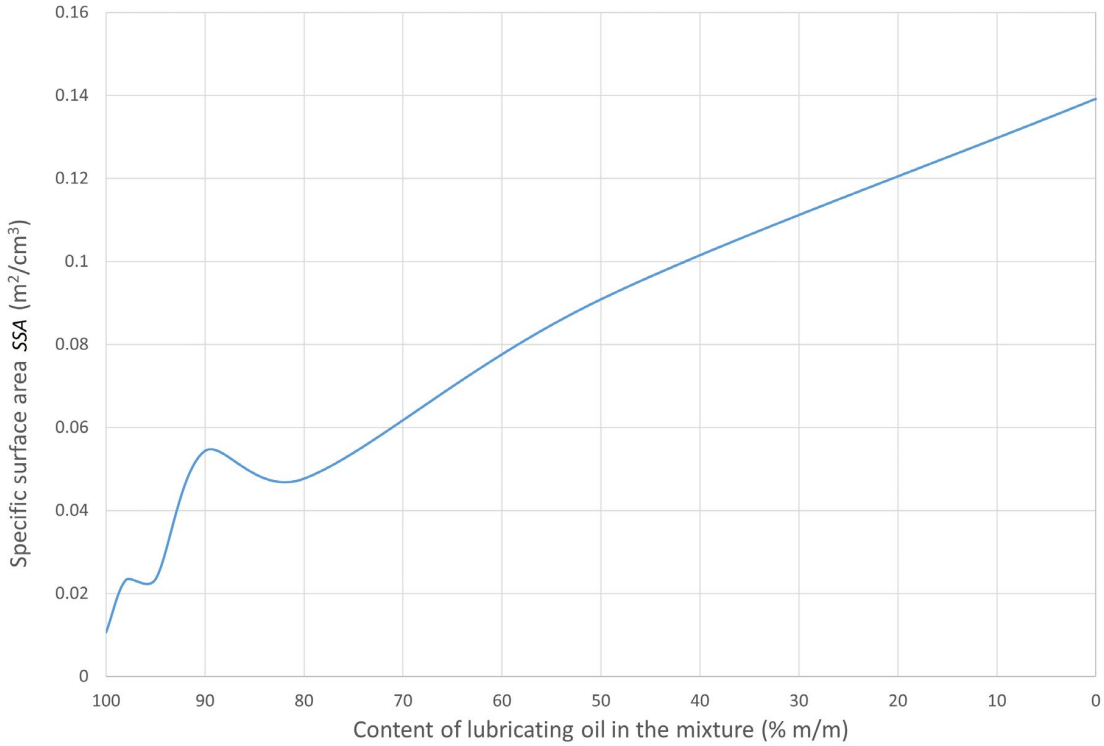

Figure 13. The specific surface area occupied by particles of mechanically generated oil mist of SAE 40 and diesel oil mixtures.

For the *SSA* and lubricating oil concentration values in the diesel oil mixture, the Pearson linear correlation coefficient was –0.974, indicating a very high negative correlation, which indicated an *SSA* increase with a decrease in lubricating oil levels in the mixture. In this case, the *SSA* increase reflects the diesel oil's effect on the total droplet surface increase in the mist.

Droplet diameters (distribution percentiles) with shares >10%, 50%, and 90% of the oil mist mixture volume are shown in Figure 14. These percentiles show slight fluctuations for diesel oil mixtures from 0–5% m/m. For diesel oil levels above 5%, the percentiles of droplet size volume distributions decrease up to 100% m/m of diesel oil. Figure 15 shows the span of the volumetric distribution of *SPAN* droplet sizes in oil mixtures for all measurements. *SPAN* values ranged from 0.5 to 3.2 and increased with added diesel oil.

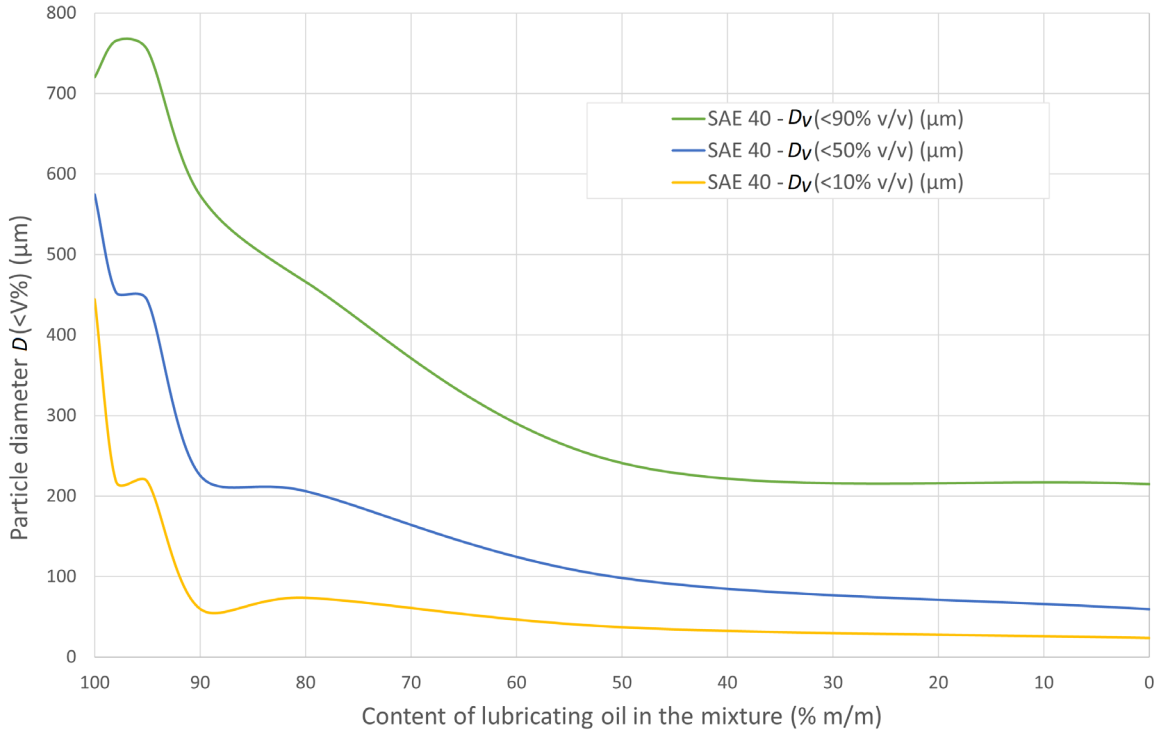

Figure 14. Droplet diameters >10%, 50%, and 90% by volume of SAE 40 and diesel oil mists.

Changes in the D_v value for mixtures directly confirm the increase in droplets with smaller and smaller diameters, along with the decrease in the lubricating oil levels in the oil mist. The correlations of these relationships are D_v(<10% v/v)—0.627, D_v(<50% v/v)—0.803 i D_v(<90% v/v)—0.890. These correspond to a high correlation for D_v(<10% v/v) and very high correlations for D_v(<50% v/v) and D_v(<90% v/v).

Increases in the span of the droplet diameter distribution in the suspension was observed. Bernoulli's principle partly explains these results—the change in the flow velocity of a given liquid from a nozzle of a given atomizer is inversely proportional to the square root of the sprayed liquid density [88]. This relationship specifies that as the density of the sprayed liquid decreases, the flow rate of the liquid from the nozzle increases in the square. An increase in the speed of the liquid flowing out of the nozzle increases the share of aerodynamic forces, forming vortices and wave deformations of the stream. All these factors increase the atomization of the spray [114]. The Bernoulli equation applies to idealized conditions in which the density of the fluid during the flow is constant, regardless of pressure changes in the flow (incompressible fluid). In fact, we are dealing with a compressible liquid.

As a supplement to the droplet volume distribution percentiles for D_v(<10% v/v), D_v(<50% v/v), and D_v(<90% v/v), the mean Sauter diameters $D_{[3,2]}$ and De Brouckere diameters $D_{[3,2]}$ were determined. Figure 16 shows those values. Diameter changes

correspond to the volume distribution percentiles of droplet sizes. Apart from insignificant fluctuations observed in diesel oil levels up to 20% m/m, the average Sauter and De Brouckere diameters decreased over all concentrations. The diameter change correlations with lubricating oil levels were 0.633 for $D_{[3,2]}$ and 0.818 for $D_{[4,3]}$, high and very high correlations, respectively.

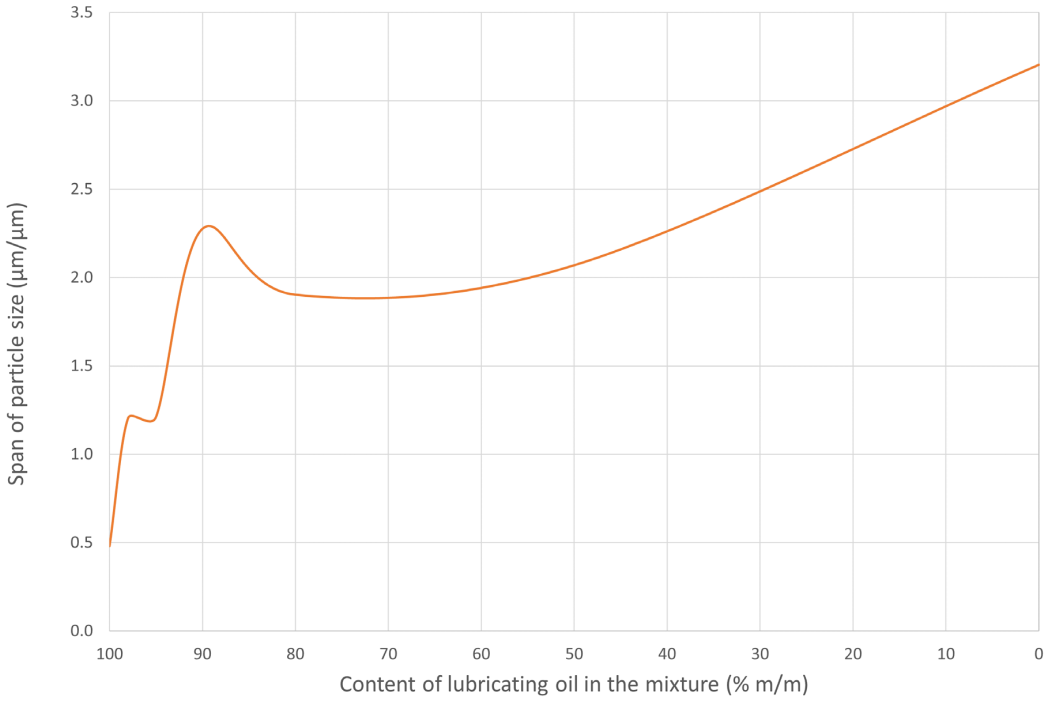

Figure 15. The span of the volumetric droplet size distribution of oil mist mixtures of SAE 40 and diesel oils.

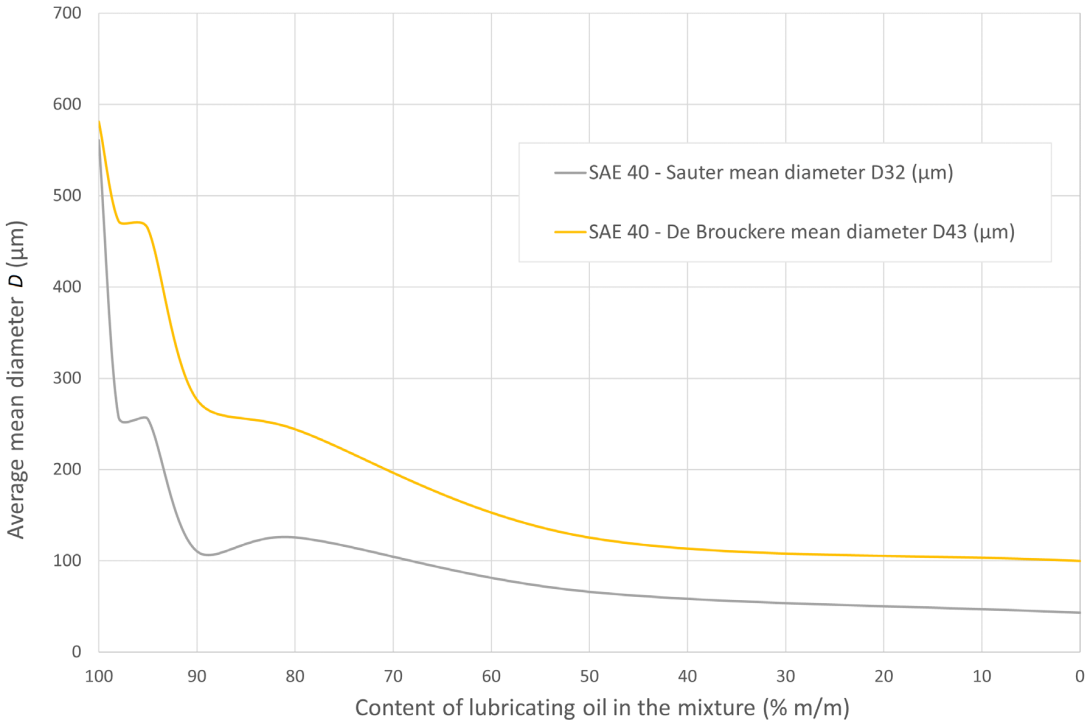

Figure 16. The mean Sauter and De Brouckere diameters of mechanically generated oil mist droplets of SAE 40 and diesel oil mixtures.

Figure 17 shows the percentage share of droplets with diameters less than or equal to 5 µm in the atomized volume %$V(D)$ and mass %$m(D)$ of the oil mist. Those results aligned with those presented in Figures 14–16. Decreases in the suspension droplet diameters in individual volume fractions and decreases in the average droplet diameter increased the percentage share of droplets with smaller and smaller diameters. For droplet diameters ≤5 µm, ignoring slight fluctuations of diesel oil concentrations above 20% m/m, changes showed increased character over the entire concentration range.

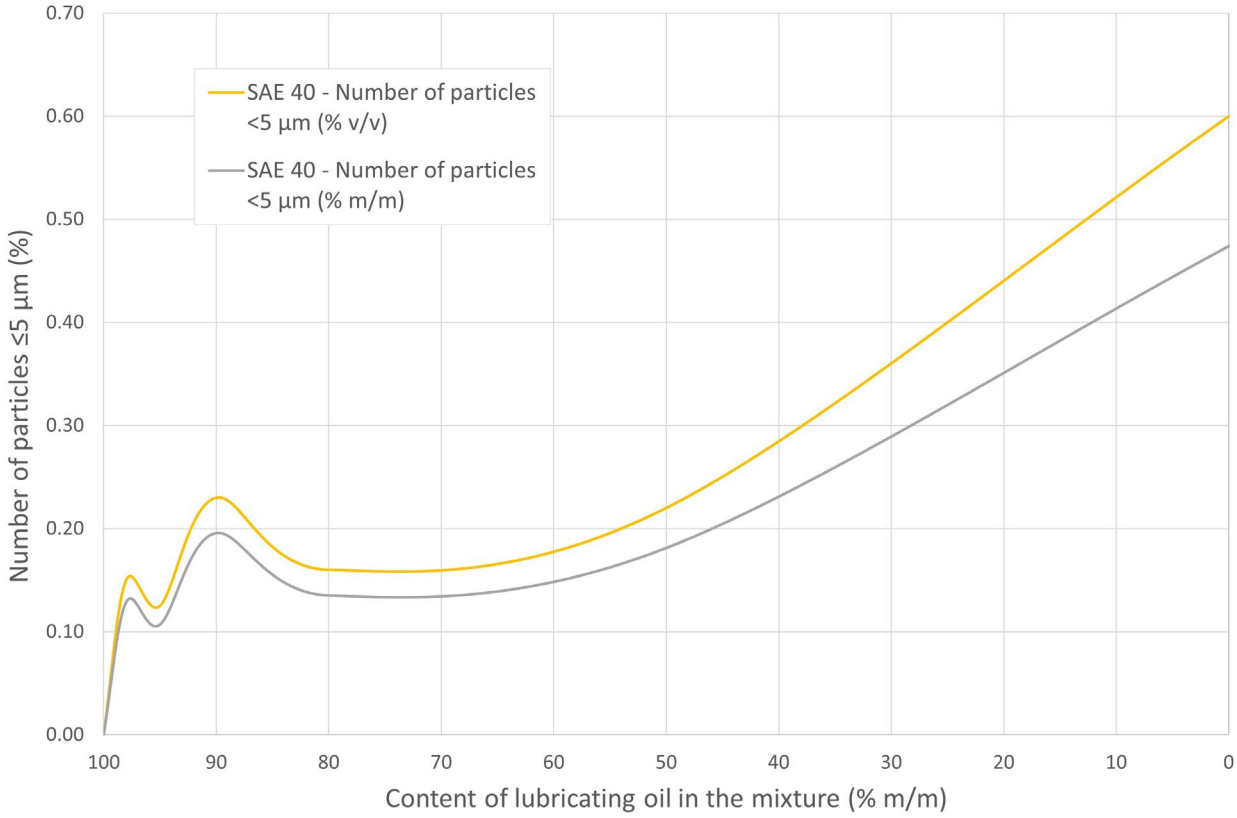

Figure 17. The number of droplets with diameters ≤5 µm in a mechanically generated oil mist of SAE 40 and diesel oil mixtures.

Results indirectly showed that diesel oil dilution in the crankcase can be a problem for engine operation and can indirectly generate a risk of explosion or intensify engine component wear, contrary to what CIMAC presented [30].

The correlation between %$V(D)$ and %$m(D)$ values and the mixture composition used to generate the oil mist was negative in this case, i.e., as pure oil concentrations dropped, the share of droplets with diameter ≤5 µm in the generated oil mist rose. The Pearson correlations (very high) for pure lubricating oil levels in mixtures with diesel oil were –0.922 for %$V(D)$ and −0.910 for %$m(D)$.

The histograms listed in Appendix B are a part of reports generated by software that supports the measuring device. The small height of the bars in the histogram for droplets with a diameter below 5 µm results from the low proportion of these droplets in the entire volume of the tested oil mist. As seen in Figure 17, they are much smaller than the concentrations of droplets with sizes above 100 µm, and even 10 µm (over 5% m/m diesel oil in the mixture). However, on all histograms, the growing proportion of small droplets is clearly visible, with an increase in the concentration of diesel oil in the mixture with lubricating oil.

The required detailed data for the histograms are provided with the associated datasets, in which interested readers can find detailed information regarding the unit participation and cumulative participation of droplets of different sizes. Droplet size distributions (de-

spite their similarity at first glance) are not normal distributions, as both the logarithmic scale and the asymmetry of the histograms with respect to the mode contradict this notion. Moreover, the mode of the normal distribution always occurs for the value of the independent variable, where the distribution's cumulative function (here, cumulative volume) equals 0.5 (here, 50%). In each of the seven histograms, the independent variable (here, particle diameter) for the mode and the cumulative function does not overlap—hence, these are not normal distributions. The most commonly used distribution for characterizing the size of droplets in sprays is the Rosin-Rammler distribution [17], which could also be applied in this case. This distribution is a form of the Weibull distribution. The authors did not fit a statistical distribution, nor did they determine its parameters because, in our opinion, the specific indicators presented in this paper can better describe the issues addressed in the article, including our main focus of interest. The latter was the participation of droplets with the smallest diameters in the oil mist and the change in this participation relative to changes in the mixture's composition used to generate the mist.

4. Conclusions

These results confirmed the hypothesis that increased contamination of a lubricating oil with diesel oil increased the share of droplets with smaller diameters in the generated oil mist. The liquid chemical composition of the mixture also influenced the increase in droplets with smaller diameters in the spray. This relates to increased volatility from additional hydrocarbons with shorter carbon chains [115,116] and decreased viscosity (lower friction forces inside the sprayed liquid) relative to pure lubricating oil [88].

A relatively small number of droplets with diameters <5 μm in the mist volume resulted from mechanical oil mist generation (relative to thermal generation). However, when evaluating changes in the indices describing droplet size distributions (a comparative assessment of relative values), more droplets with smaller and smaller diameters in the suspension were observed with additional diesel oil in the mixtures.

Due to the detailed experimental data indicated in the article and associated datasets, it can be assumed that the experiment can be successfully repeated and extended to other mixtures (other types/grades of lubricating oils and fuels).

Future work should focus on analogous tests for thermally generated oil mists and a way to combine both methods, which may require the construction of a dedicated oil mist generator, especially for these tests. In addition, future work should test for other potential contaminants in engine lubricating oils, such as residual fuels, refuse-derived fuels, and biofuels of various origins. Such research could broaden the understanding of lubricating oil components on engine component wear and the emergence of explosion and fire hazards during operation.

Building a statistical model of the droplet size (i.e., represented by its diameter) depending on the mixture composition and the spray production parameters may also be the subject of future research.

Author Contributions: Conceptualization, L.C.; methodology, L.C. and K.G.; software, L.C., M.S., K.G. and O.K.; validation, L.C. and K.G.; formal analysis, L.C., M.S., K.G. and O.K.; investigation, L.C., M.S., K.G. and O.K.; resources, L.C. and M.S.; data curation, L.C. and M.S.; writing—original draft preparation, L.C., M.S., K.G. and O.K.; writing—review and editing, L.C., M.S., K.G. and O.K.; visualization, L.C. and M.S.; supervision, L.C.; project administration, L.C.; funding acquisition, L.C. All authors have read and agreed to the published version of the manuscript.

Funding: This research was funded by the Ministry of Science and Higher Education (MEiN) of Poland, grant number 1/S/KPBMiM/23. APC was covered by MDPI.

Data Availability Statement: All data are available in this paper and the dataset: Chybowski, L. Lube oil—diesel oil mixes—dataset; 2022, Ver. 3, DOI: 10.17632/scbx3h2bmf.3. Dataset is available at https://data.mendeley.com/datasets/scbx3h2bmf/3 (accessed on 10 April 2023) [92]. Chybowski, L.; Szczepanek, M.; Gawdzińska, K.; Klyus, O. Morphology of oil mechanically generated mist from mixes of grade SAE 40 lubricating oil and diesel oil; 2023, Ver. 1, DOI: 10.17632/wtp6z3skgm.1.

Dataset is available at https://data.mendeley.com/datasets/wtp6z3skgm (accessed on 10 April 2023) [93].

Acknowledgments: Laboratory tests were performed on behalf of the authors at the Center for Testing Fuels, Working Fluids, and Environmental Protection (CBPCRiOS) of the Maritime University of Szczecin. The authors would like to thank Magdalena Szmukała and Barbara Żurańska for their technical support.

Conflicts of Interest: The authors declare no conflict of interest. The funders had no role in the study's design; in the collection, analyses, or interpretation of data; in the writing of the manuscript; or in the decision to publish the results.

Abbreviations

%m(D)	the mass percentage of droplets with a diameter equal to or smaller D
%V(D)	percentage by volume of droplets with a diameter equal to or smaller D
A	total area of particles
CIMAC	the International Council on Combustion Engines
D	particle diameter
d_0	atomizer slot diameter
$D_{[3,2]}$	Sauter diameter
$D_{[4,3]}$	De Brouckere diameter
D_S, $D_{[2,0]}$	Surface diameter
D_V	percentile of the volume distribution of droplet size (diameter)
D_{Vol}, $D_{[3,0]}$	volume diameter
F	the amount of laser light reaching the beam power detector
F_0	the amount of laser light emitted by the transmitter
HFFR	high-frequency reciprocating rig
i	number of the size class with upper particle size x_i
IACS	International Association of Classification Societies
IGC	International Gas Carrier Code
IGF	International Code of Safety for Ship Using Gases or Other Low-flashpoint Fuels
IMO	International Maritime Organization
l_0	atomizer channel length
n	the number of particles in i-th size class
N	the number of size classes
R	the residual value of the fit between the measured and calculated scattering data
r_{XY}	Pearson's linear correlation coefficient of X and Y variables
RMG	Regulation of the Minister of Economy on quality requirements for liquid fuels
SAE	Society of Automotive Engineers
SAE 40	viscosity grades of lubricating oils according to the SAE J300-2021 standard
SHD	engine shut down
SLD	engine slow down
SOLAS	International Convention for the Safety of Life at Sea
SPAN	the relative width of the statistical distribution of droplet sizes in the mixture volume
SSA	the specific surface area of the oil mist
t	time, moment of data recording
T	light transmission coefficient
V	the total volume of particles
X, Y	variables subjected to statistical analysis
ρ	density of the tested oil mixture
σ_X, σ_Y	standard deviation of variables X and Y

Appendix A. Tables

Table A1. The required oil properties in the case of SAE 40 viscosity grade following the SAE J300-2021 engine oil viscosity classification (based on [81]).

Parameter [b]	**Min. Low-Shear-Rate Kinematic Viscosity (mm^2/s)** [a] **at 100 °C**	**Max. Low-Shear-Rate Kinematic Viscosity (mm^2/s)** [a] **at 100 °C**	**Min. High-Shear-Rate Viscosity (mPa·s)** [a] **at 150 °C**
Test methods and references	ASTM D445 or ASTM D7042 [c]	ASTM D445 or ASTM D7042 [c]	ASTM D4683, ASTM D4741, ASTM D5481, or CEC L-36-90
SAE 40	12.5	<16.3	3.7

[a]—1 mPa·s = 1 cP; 1 mm^2/s = 1 cSt. [b]—All values are critical specifications as defined by ASTM D3244 [c]—ASTM D445 or ASTM D7042 bias corrected to ASTM D445.

Table A2. Characteristics of CF oils according to the API classification (based on [58,87]).

Category	**Engine Types**	**Service Characteristics**	**Backward API Category Compatibility**
CF	Category of engine oils intended for use in engines with direct injection and other compression ignition engines. Intended for off-road engines that use fuel containing more than 0.5% sulfur.	Provides control of: piston deposits, piston, ring, and liner scuffing, wear and corrosion of copper-containing bearings.	CD

Appendix B

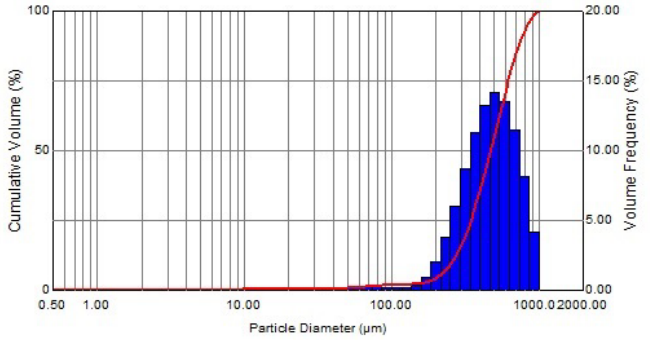

SAE 40—100%, DO—0%

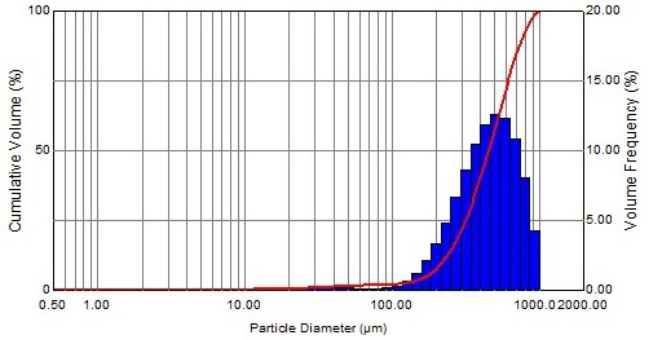

SAE 40—98% m/m, DO—2% m/m

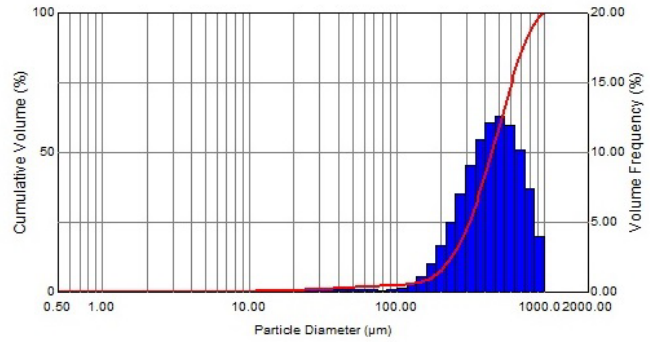

SAE 40—95% m/m, DO—5% m/m

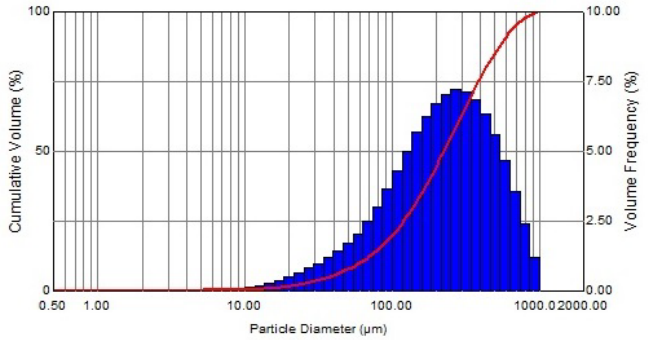

SAE 40—90% m/m, DO—10% m/m

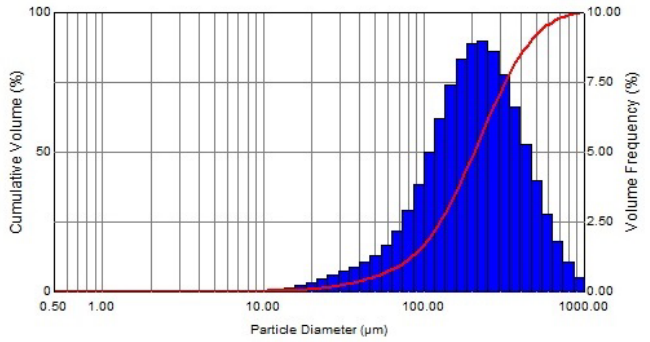

SAE—40 80% m/m, DO—20% m/m

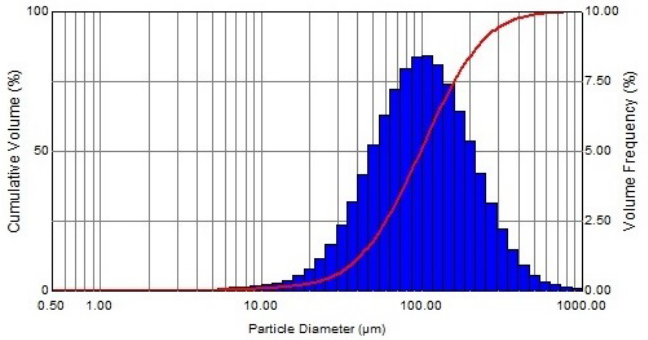

SAE 40—50% m/m, DO—50% m/m

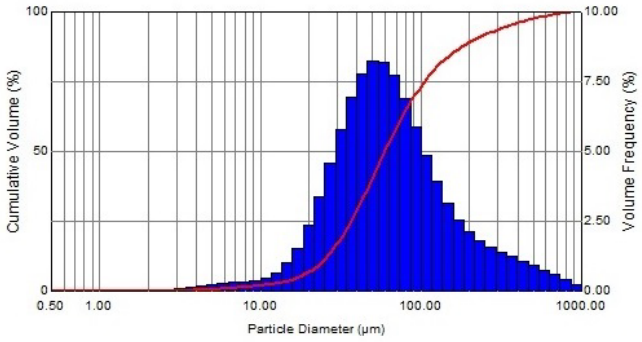

SAE 40—0%, DO—100%

Figure A1. Droplet Size Distribution of the Oil-Fuel Mixture for Measurements with the Slightest Error.

References

1. Chybowski, L.; Jakubowski, A.; Żółkiewski, S. Analysis of the Relationship between Selected Ship and Propulsion System Characteristics and the Risk of Main Engine Turbocharger Explosion. *J. Mar. Sci. Eng.* **2023**, *11*, 360. [CrossRef]
2. Chybowski, L.; Twardochleb, M.; Wiśnicki, B. Multi-criteria Decision making in Components Importance Analysis applied to a Complex Marine System. *Nase More* **2016**, *63*, 264–270. [CrossRef]
3. Herdzik, J. Problems of propulsion systems and main engines choice for offshore support vessels. *Sci. J. Marit. Univ. Szczec.* **2013**, *36*, 45–50.
4. Sawicka, M.; Szczepanek, M. Legal conditions regarding the energy efficiency of fishing vessels. *Sci. J. Marit. Univ. Szczec.* **2013**, *36*, 170–174.
5. Borkowski, J.; Kowalak, T.; Myśków, P. Vessel main propulsion engine performance evaluation. *J. KONES* **2012**, *19*, 53–60. [CrossRef]
6. Kazienko, D.; Chybowski, L. Instantaneous Rotational Speed Algorithm for Locating Malfunctions in Marine Diesel Engines. *Energies* **2020**, *13*, 1396. [CrossRef]
7. Ubowska, A.; Szczepanek, M. Engine rooms fire safety – fire-extinguishing system requirements. *Sci. J. Marit. Univ. Szczec.* **2016**, *48*, 51–57. [CrossRef]
8. Krystosik-Gromadzińska, A. Engine room fire safety. *Sci. J. Marit. Univ. Szczec.* **2016**, *47*, 29–35. [CrossRef]
9. Chybowska, D.; Chybowski, L.; Guze, S.; Wilczyński, P. A method for determining critical events during large disasters of production platforms. *J. Loss Prev. Process Ind.* **2021**, *72*, 104528. [CrossRef]
10. MAN B&W. *Diesel A/S Crankcase Explosions in Two-Stroke Diesel Engines*; MAN Burmeister and Wain: København, Denmark, 2002.
11. Chybowski, L. *Eksplozje w Skrzyniach Korbowych Silników Okrętowych—Przyczyny, Zapobieganie i Minimalizacja Skutków*; Akademia Morska w Szczecinie: Szczecin, Poland, 2022.
12. Rattenbury, N. Crankcase expolsions—A historical review—Where we are today. In *Crankcase Explosions*; IMAREST: London, UK, 2002; pp. 3–13.
13. Rickaby, P.; Rattenbury, N.; Uebel, H.; Ohlsen, E.; Evans, D.J.; Milne, A.M.; Rose, D.J.; Heikamp, W.; Bowen, P.; Brunk, H.; et al. *Crankcase Explosions*; IMAREST: London, UK, 2002.
14. Burgoyne, J.; Newitt, D. Crankcase explosions in marine engines. *J. Am. Soc. Nav. Eng.* **1956**, *68*, 122–128.
15. Chybowski, L.; Wiaterek, D.; Jakubowski, A. The Impact of Marine Engine Component Failures upon an Explosion in the Starting Air Manifold. *J. Mar. Sci. Eng.* **2022**, *10*, 1850. [CrossRef]
16. Zhou, S.; Wang, Z.; Li, Q. A conceptual framework integrating numerical simulation with system theory based method for quantitative explosion process hazard analysis. *Process Saf. Environ. Prot.* **2022**, *166*, 202–211. [CrossRef]
17. Shamsuddin, D.A.; Fekeri, A.M.; Muchtar, A.; Khan, F.; Khor, B.; Lim, B.; Rosli, M.; Takriff, M. Computational fluid dynamics modelling approaches of gas explosion in the chemical process industry: A review. *Process Saf. Environ. Prot.* **2023**, *170*, 112–138. [CrossRef]
18. Wu, F.; Yu, H.; Pan, X.; Zang, X.; Hua, M.; Wang, H.; Jiang, J. Experimental study of methanol atomization and spray explosion characteristic under negative pressure. *Process Saf. Environ. Prot.* **2022**, *161*, 162–174. [CrossRef]
19. Minkhorst, J. *Crank Case Explosions in Diesel Engines, Studiecentrum TNO Voor Scheepsbouw en Navigatie*; Maritime University of Szczecin: Delft, The Netherlands, 1957.
20. Eckhoff, R. *Explosion Hazards in the Process Industries*; Elsevier: Houston, TX, USA, 2005. [CrossRef]
21. Valčić, M. The Learning Resource for Marine Engineers www.marinediesels.co.uk, Warshash Maritime Academy, Warsash, Rjeka, n.d. Available online: https://www.scribd.com/doc/27517784/Marine-Diesels-Co-Uk (accessed on 30 April 2021).
22. The Hong Kong Special Administrative Region. *Report of Investigation into the Engine Room Fire on Board Hong Kong Registered M.T. "An Tai Jiang" on 9 January 2009*; Marine Department. Marine Accident Investigation Section: Hong Kong, China, 2009.
23. Cicek, K.; Celik, M. Application of failure modes and effects analysis to main engine crankcase explosion failure on-board ship. *Saf. Sci.* **2013**, *51*, 6–10. [CrossRef]
24. Wang, Z.-L.; You, J.-X.; Liu, H.-C.; Wu, S.-M. Failure Mode and Effect Analysis using Soft Set Theory and COPRAS Method. *Int. J. Comput. Intell. Syst.* **2017**, *10*, 1002. [CrossRef]
25. Ünver, B.; Gürgen, S.; Sahin, B.; Altın, İ. Crankcase explosion for two-stroke marine diesel engine by using fault tree analysis method in fuzzy environment. *Eng. Fail. Anal.* **2019**, *97*, 288–299. [CrossRef]
26. Wiaterek, D.; Chybowski, L. Assessing the topicality of the problem related to the explosion of crankcases in marine main propulsion engines (1972–2018). *Sci. J. Marit. Univ. Szczec.* **2022**, *71*, 33–40.
27. Ehsan, M.; Rahman, M.; Hasan, M. Effect of Fuel Adulteration on Engine Crankcase Dilution. *J. Mech. Eng.* **2010**, *41*, 114–120. [CrossRef]
28. Chybowski, L. Study of the Relationship between the Level of Lubricating Oil Contamination with Distillation Fuel and the Risk of Explosion in the Crankcase of a Marine Trunk Type Engine. *Energies* **2023**, *16*, 683. [CrossRef]
29. Ferguson, G. *Diesel Engine Crankcase Explosion Investigation*; SAE Tech. Pap. 510104; SAE: Warrendale, PA, USA, 1951; pp. 1–28. [CrossRef]
30. CIMAC. *Guideline on the Relevance of Lubricationt Flash Point in Connection with Crankcase Explosions*; CIMAC Working Group 8 "Marine Lubricants": Frankfurt, Germany, 2013.

31. Graddage, M. Crankcase Explosions—Detection or Prevention ? In *Crankcase Explosions*; IMAREST: London, UK, 2002; pp. 126–147.
32. Technomics International. Case Study—Fuel Dilution of Engine Oil in Locomotives. 2022. Available online: https://www.techenomics.net/case-studies/fuel-dilution-engine-oil/ (accessed on 8 June 2022).
33. Porowski, R.; Kobylińska, A.; Dziechciarz, A. Kalbarczyk-Jedynak, Doświadczalne i numeryczne badania temperaturowych granic palności propanoli i ich mieszanin z olejem napędowym. *Przem. Chem.* **2019**, *1*, 44–48. [CrossRef]
34. Krupowies, J. *Badania Zmian Parametrów Fizykochemicznych Silnikowych Olejów Smarowych Eksploatowanychna Statkach Polskiej Żeglugi Morskiej, Studia Nr*; Wyższa Szkoła Morska w Szczecinie: Szczecin, Poland, 1996.
35. Chybowski, L. The Initial Boiling Point of Lubricating Oil as an Indicator for the Assessment of the Possible Contamination of Lubricating Oil with Diesel Oil. *Energies* **2022**, *15*, 7927. [CrossRef]
36. MDPI. Peer-Review Record. Study of the Relationship between the Level of Lubricating Oil Contamination with Distillation Fuel and the Risk of Explosion in the Crankcase of a Marine Trunk Type Engine. *Rev. Rep.* **2023**, *16*, 683. Available online: https://www.mdpi.com/1996-1073/16/2/683/review_report (accessed on 16 February 2023).
37. IACS. *Requirements Concerning Machinery Installations*; International Association of Classification Societies: London, UK, 2016.
38. IMO. *SOLAS—Consolidated Edition 2020*; International Maritime Organization: London, UK, 2020.
39. Nozdrzykowski, K.; Adamczak, S.; Grządziel, Z.; Dunaj, P. The Effect of Deflections and Elastic Deformations on Geometrical Deviation and Shape Profile Measurements of Large Crankshafts with Uncontrolled Supports. *Sensors* **2020**, *20*, 5714. [CrossRef] [PubMed]
40. Nozdrzykowski, K. Applying Harmonic Analysis in the Measurements of Geometrical Deviations of the Crankshafts – Selecting Support Conditions. *MAPE* **2018**, *1*, 191–195. [CrossRef]
41. Nozdrzykowski, K. Error Analysis of Graphical Interpretation of Circularity Profile. *Sci. J. Marit. Univ. Szczec.* **2006**, *10*, 329–338.
42. Babrauskas, V. *Ignition Handbook*; Society of Fire Protection Engineers: Gaithersburg, MD, USA, 2003.
43. FireNet Special Interest Network. Maritime Case Histories. 2009. Available online: http://fire.org.uk/marine/incidents.htm (accessed on 24 November 2009).
44. Bistrović, M.; Ristov, P.; Komorčec, D. Prediction of potential fire hot spots by using a model based on a computerized real – time view with IR cameras on ships. *Sci. J. Marit. Univ. Szczec.* **2017**, *50*, 23–29. [CrossRef]
45. Bonisławski, M.; Hołub, M.; Borkowski, T.; Kowalak, P. A Novel Telemetry System for Real Time, Ship Main Propulsion Power Measurement. *Sensors* **2019**, *19*, 4771. [CrossRef]
46. DNV-GL. *Rules for Classification. Ships Part 5 Ship Types Chapter 7 Liquefied Gas Tankers*; DNV-GL: Oslo, Norway, 2018.
47. Win, G.D. *2-Stroke Dual-Fuel Safety Concept*; Winterthur Gas & Diesel: Winterthur, Switzerland, 2021.
48. Ślesicki, O. *Analiza Zabezpieczeń Przeciwpożarowych i Przeciwwybuchowych Stosowanych w Silnikach Sulzer Serii RTA, Praca Dyplomowa Inżynierska*; Akademia Morska w Szczecinie, Wydział Mechaniczny ITESO: Szczecin, Poland, 2009.
49. Hamied, M. *Effectiveness of Crankcase-Oil Mist Detectors*; University College of Southeast Norway, Bø, Kongsberg: Porsgrunn, Norway, 2016.
50. Piotrowski, I.; Witkowski, K. *Eksploatacja Okrętowych Silników Spalinowych*; Akademia Morska w Gdyni: Gdynia, Poland, 2005.
51. SAB. *Operation Manual Part-No. 10980. Version 2.4, 11/2015 VISATRON®Oil Mist Detectors VN115/93, VN116/93, VN215/93, Schaller Automation*; SAB: Blieskastel/Saarland, Germany, 2015.
52. Wu, D.; Zhao, P.; Spitzer, S.; Krietsch, A.; Amyotte, P.; Krause, U. A review on hybrid mixture explosions: Safety parameters, explosion regimes and criteria, flame characteristics. *J. Loss Prev. Process Ind.* **2023**, *82*, 104969. [CrossRef]
53. Islam, S. Crankcase Explosion Mechanism. 2014. Available online: https://www.slideshare.net/saiful12345660/crankcase-explosion-mechanism (accessed on 21 March 2021).
54. Schaller Automation. *Possibiliteies and Limits of the Prevention of Damage through the Monitoring of Crankcase Compartments*; Schaller Automation: Blieskastel, Germany, 2009.
55. Schaller Automation. Crankcase Explosion. 2020. Available online: https://schaller.sg/product/crankcase-explosion/ (accessed on 20 June 2022).
56. Wiaterek, D.; Chybowski, L. Comparison of selected models useful in ranking the root causes of explosions in marine engine crankcases. *Sci. J. Marit. Univ. Szczec.* **2022**, *72*, 77–85.
57. Brünnet, H.; Reppekus, D.; Theobald, M.; Kornatz, G. Formation and avoidance of crankcase explosions in large oil, dual-fuel and gas engines. In Proceedings of the 5th Rostock Large Engine Symposium, Rostock, Germany, 13–14 September 2018; pp. 280–297.
58. El-Zahlanieh, S.; Jean, A.; Vignes, A.; Dufaud, O. A sneak peek into the phenomenology of fuel mist explosions: The key role of vapor fractions. *J. Loss Prev. Process Ind.* **2023**, *83*, 105029. [CrossRef]
59. Krystosik-Gromadzińska, A. Affordable hybrid thermography for merchant vessel engine room fire safety. *Sci. J. Marit. Univ. Szczec.* **2019**, *57*, 21–26. [CrossRef]
60. Herdzik, J. Remarks of the FMEA procedures for ships with dynamic positioning systems. *Zesz. Nauk. Akad. Mor. W Gdyni* **2015**, *91*, 47–53.
61. Marine Diesels. Crankcase Explosions—Oil Mist Detection, (n.d.). Available online: http://www.marinediesels.info/members/CrankcaseExplosions/Oil_Mist_Detection.htm (accessed on 17 March 2021).
62. Burgoyne, J.; Cohen, L. The effect of drop size on flame propagation in liquid aerosols. *Proc. R. Soc. London. Ser. A. Math. Phys. Sci.* **1954**, *225*, 375–392. [CrossRef]

63. Nozdrzykowski, K.; Grządziel, Z.; Grzejda, R.; Warzecha, M.; Stępień, M. An Analysis of Reaction Forces in Crankshaft Support Systems. *Lubricants* **2022**, *10*, 151. [CrossRef]
64. Nozdrzykowski, K.; Grządziel, Z.; Dunaj, P. Determining geometrical deviations of crankshafts with limited detection possibilities due to support conditions. *Measurement* **2022**, *187*, 110430. [CrossRef]
65. Łosiewicz, Z. Bezpieczeństwo pracy na morzu—Weryfikacja kompetencji załóg w realnych warunkach zagrożenia pożarowego statku. *Autobusy* **2016**, *6*, 260–263.
66. Krystosik-Gromadzińska, A. *Wybrane Problemy Kształtowania Bezpieczeństwa Pożarowego Siłowni Okrętowej*; Wydawnictwo Uczelniane Zachodniopomorskiego Uniwersytetu Technologicznego w Szczecinie: Szczecin, Poland, 2020.
67. Herdzik, J. ISM Code on Vessels with or Without Impact on a Number of Incidents Threats. *J. KONES.* **2019**, *26*, 53–59. [CrossRef]
68. Bejger, A.; Chybowski, L.; Gawdzińska, K. Utilising elastic waves of acoustic emission to assess the condition of spray nozzles in a marine diesel engine. *J. Mar. Eng. Technol.* **2018**, *17*, 153–159. [CrossRef]
69. Klyus, O.; Zamiatina, N. Residual fuel atomization process simulation. *Combust. Engines* **2017**, *169*, 108–112. [CrossRef]
70. Dyson, C.; Priest, M.; Lee, P. Simulating the Misting of Lubricant in the Piston Assembly of an Automotive Gasoline Engine: The Effect of Viscosity Modifiers and Other Key Lubricant Components. *Tribol. Lett.* **2022**, *70*, 49. [CrossRef]
71. Avergård, P.; Lindström, F. *Modelling of Crankcase Gas Behaviour in a Heavy-Duty Diesel Engine*; Lund Institute of Technology: Lund, Sweden, 2003.
72. Berthome, V.; Chalet, D.; Hetet, J.-F. Consequence of Blowby Flow and Idling Time on Oil Consumption and Particulate Emissions in Gasoline Engine. *Energies* **2022**, *15*, 8772. [CrossRef]
73. HHerbst, M.; Priebsch, H. Simulation of Piston Ring Dynamics and Their Effect on Oil Consumption. In Proceedings of the SAE 2000 World Congress, Detroit, MI, USA, 6–9 March 2000; pp. 1–14. [CrossRef]
74. Shell, P. Relationship Between Oil Consumption, Deposit Formation and Piston Ring Motion for Single-Cylinder Diesel Engines. In Proceedings of the International Congress & Exposition, Detroit, MI, USA, 24–28 February 1992; pp. 1–15. [CrossRef]
75. Huizenga, P. What Does the 2nd Piston Ring Do? Purpose and Function Explained! Wiseco. 2020. Available online: https://wiseco.com/blog/2nd-ring-purpose-and-function-explained (accessed on 21 February 2022).
76. Xiong, H.; Sun, W. Investigation of Droplet Atomization and Evaporation in Solution Precursor Plasma Spray Coating. *Coatings* **2017**, *7*, 207. [CrossRef]
77. Li, T.; Nishida, K.; Hiroyasu, H. Droplet size distribution and evaporation characteristics of fuel spray by a swirl type atomizer. *Fuel* **2011**, *90*, 2367–2376. [CrossRef]
78. SAB. *Operation Manual Version 1.2 Visatron®VN301plus/VN301plusEX IACS UR M67/M10 Type Approved*; Schaller Automation: Blieskastel, Germany, 2015; 301p.
79. Concept Smoke Systems. Concept Oil Mist Generator (OMG). 2023. Available online: https://www.concept-smoke.co.uk/products/concept_omg.aspx (accessed on 25 February 2023).
80. Hyrouki, H.; Toshikazu, K. Fuel droplet size distribution in diesel combustion chamber. *Bull. JSME* **1976**, *19*, 1064–1072.
81. Society of Automotive Engineers. *SAE J300-2021. Engine Oil Viscosity Classification*; SAE International: Warrendale, PA, USA, 2021.
82. API. Engine Oil Guide. 2013. Available online: https://www.api.org/~/media/files/certification/engine-oil-diesel/publications/mom_guide_english_2013.pdf (accessed on 26 February 2023).
83. Oleje-Smary. AGIP Cladium 120 SAE 40 CD. 2022. Available online: https://oleje-smary.pl/pl/p/AGIP-Cladium-120-SAE-40-CD-20-litrow/188 (accessed on 12 July 2022).
84. Orlen, S.P.; Napędowy, O. Ecodiesel Ultra B, D, F, Olej napędowy arktyczny klasy 2, Efecta Diesel B,D,F, Verva ON B,D,F, PKN Orlen S.A., Płock, 2022. Available online: https://www.orlen.pl/pl/dla-biznesu/produkty/paliwa/oleje-napedowe/ekodiesel-ultra-klasa-2 (accessed on 1 June 2022).
85. Minister Gospodarki RP. *Rozporządzenie Ministra Gospodarki z Dnia 9 Października 2015 r. w Sprawie Wymagań Jakościowych Dla Paliw Ciekłych*; Ministerstwo Gospodarki RP: Warszawa, Poland, 2015. Available online: https://isap.sejm.gov.pl/isap.nsf/download.xsp/WDU20150001680/O/D20151680.pdf (accessed on 1 April 2023).
86. PKN Orlen, S.A. ZN-ORLEN-5 Manufacturer Standard—Przetwory naftowe. Olej napędowy EFECTA DIESEL; PKN Orlen S.A.: Płock, Poland, 2019.
87. *ISO 8217:2017*; Petroleum products—Fuels (class F)—Specifications of Marine Fuels. 6th ed. ISO: Geneva, Switzerland, 2017.
88. Piotrowski, I.; Witkowski, K. *Okrętowe Silniki Spalinowe*, 3rd ed.; Trademar: Gdynia, Poland, 2013.
89. Kowalak, P.; Myśków, J.; Tuński, T.; Bykowski, D.; Borkowski, T. A method for assessing of ship fuel system failures resulting from fuel changeover imposed by environmental requirements. *Eksploat. I Niezawodn. Maint. Reliab.* **2021**, *23*, 619–626. [CrossRef]
90. Oleje-Smary. AGIP Cladium 120 SAE 30 CD. 2022. Available online: https://oleje-smary.pl/pl/p/AGIP-Cladium-120-SAE-30-CD-20-litrow/186 (accessed on 12 July 2022).
91. ITALCO (Far East) Pte Ltd. *Product Data Sheet—Eni Cladium 120 (Series)*; ITALCO: Singapore, 2017.
92. Chybowski, L. Lube Oil—Diesel Oil Mixes—Dataset. 2022. Available online: https://doi.org/10.17632/scbx3h2bmf.3 (accessed on 1 April 2023).
93. Chybowski, L.; Szczepanek, M.; Gawdzińska, K.; Klyus, O. Morphology of Oil Mechanically Generated Mist from Mixes of Grade SAE 40 Lubricating Oil and Diesel Oil, Dataset. 2023. Available online: https://doi.org/10.17632/wtp6z3skgm.1 (accessed on 1 April 2023).

94. Prendes-Gero, M.-B.; Álvarez-Fernández, M.-I.; Conde-Fernández, L.; Luengo-García, J.-C.; González-Nicieza, C. Experimental study of the characteristics of explosions generated by methane mixtures, as a function of the type of atmosphere and environmental conditions. *J. Loss Prev. Process Ind.* **2022**, *80*, 104878. [CrossRef]
95. Malvern Instruments. *Spraytec User Manual*; Malvern Instruments: Worcestershire, UK, 2007.
96. Mie, G. Beiträge zur Optik trüber Medien, speziell kolloidaler Metallösungen. *Ann. Phys.* **1908**, *330*, 377–445. [CrossRef]
97. Hahn, D. Light Scattering Theory. 2009 1-13. Available online: http://plaza.ufl.edu/dwhahn/RayleighandMieLightScattering.pdf (accessed on 26 February 2023).
98. Jenkins, F.; White, H. *Fundamentals of Optics, IV*; McGraw-Hill Higher Education: Boston, MA, USA, 2001.
99. Polmo. *Naprawa Samochodów Star 266*; WKiŁ: Warszawa, Poland, 1976.
100. WSK, PRW3. Próbnik Wtryskiwaczy. 2023. Available online: http://www.wsk.com.pl/wtrysk_2.html (accessed on 26 January 2023).
101. Angraini, N.; Kurniawati, A. Comparative Analysis of Fintech Software Quality Against MSMEs Using the ISO 25010:2011 Method. *Int. Res. J. Adv. Eng. Sci.* **2021**, *6*, 167–175.
102. Barlow, R.; Proschan, F. *Statistical Theory of Reliability and Life Testing: Probability Models*; Holt, Rinehart and Winston: New York, NY, USA, 1974.
103. Tian, J.; Chen, B.; Li, D. Light transmittance dynamics and spectral absorption characteristics during auxiliary cryogen spray cooling in laser dermatology. *Lasers Med. Sci.* **2022**, *37*, 2079–2086. [CrossRef]
104. Gant, S. *Generation of Flammable Mists from High Flashpoint Fluids: Literature Review*; HSE: Buxton, UK, 2013.
105. *ISO 9276-2*; Representation of Results of Particle Size Analysis—Part 2: Calculation of Average Particle Sizes/Diameters and Moments from Particle Size Distributions. ISO: Geneva, Switzerland, 2014.
106. Anton Paar, Particle Size Distribution. 2023. Available online: https://wiki.anton-paar.com/pl-pl/particle-size-distribution/ (accessed on 6 February 2023).
107. Azzopardi, B. Sauter Mean Diameter. In: A-to-Z Guid. to Thermodyn. Heat Mass Transf. Fluids Eng., Begellhouse, 2011. Available online: https://doi.org/10.1615/AtoZ.s.sauter_mean_diameter (accessed on 1 April 2023).
108. Michalska-Pożoga, I.; Szczepanek, M. Analysis of Particles' Size and Degree of Distribution of a Wooden Filler in Wood–Polymer Composites. *Materials* **2021**, *14*, 6251. [CrossRef] [PubMed]
109. Risi, A.; Sante, R.; Colangelo, G. Optical Characterization of a Diesel Spray at High Temperature and Pressure. In *XII Convegno Naz*; A.I.VE.LA: Napoli, Italy, 2004; pp. 1–13.
110. Sauter, J. *Die Grössenbestimmung von Brennstoffteilchen, Forschungsarbeiten auf dem Gebiete des Ingenieurwesens (Mitteilung aus dem Laboratorium für technische Physik der Technischen Hochschule München), Heft 279*; VDI-Verlag: Berlin, Germany, 1926.
111. Sauter, J. *Untersuchung der von Spritzvergasern Gelieten Zerstäubung, Forschungsarbeiten auf Dem Gebiete des Ingenieurwesens, Heft 312*; VDI-Verlag: Berlin, Germany, 1928.
112. United Technologies. Graviner, The MK7 Oil Mist Detector Presentation, Graviner. United Technologies: Hartford, CT, USA.
113. Stocznia Szczecińska. *Detektor o Wysokiej Czułości Typ 4 do Określania Stężenia Mgły Oplejowej. Typ Komparatorowy i Niwelacyjny*; Stocznia Szczecińska: Szczecin, Poland, 1997.
114. Włodarski, K.; Witkowski, K. *Okrętowe Silniki Spalinowe. Podstawy Teoretyczne*; Akademia Morska w Gdyni: Gdynia, Poland, 2006.
115. Włodarski, J. *Stany Eksploatacyjne Okrętowych Silników Spalinowych*; Wydawnictwo Uczelniane WSM w Gdyni: Gdynia, Poland, 1998.
116. Jääskeläinen, H. Oile Service Classifications, DieselNet Technol Guid. 2022. Available online: https://dieselnet.com/tech/lube_classifications.php (accessed on 26 February 2023).